Mercury Emissions from Volcanic Sources in Central America

By

David Skye Kushner

A Thesis submitted to the Faculty of Graduate Studies of
The University of Manitoba
In partial fulfillment of the requirements of the degree of

Master of Science

Department of Environment and Geography
University of Manitoba
Winnipeg

Abstract

Volcanoes are recognized contributors of mercury (Hg) emissions to the atmosphere; however, the amount of Hg released globally from these natural sources remains poorly constrained. To improve our understanding of volcanic Hg emissions, a multi-year suite of atmospheric, water, and ash samples were collected from Poás and Turrialba volcanoes, Costa Rica. Atmospheric sampling at Poás was conducted over two stages of volcanic activity (passive degassing and active eruption) using continuous monitoring near the crater in addition to passive and active sampling techniques within the crater. Results corroborate earlier assessments that Poás is a low Hg emitting volcano compared to Turrialba, even during active phases. A novel model of crustal Hg incorporation is proposed to explain the large global variance in volcanic plume Hg concentrations in relationship to eruption frequency. Based on the model, a new global volcanic Hg flux is estimated to be 30 ± 39 t a^{-1} for 2006–2015.

Acknowledgements

I would like to thank my mother, Linda Cohen, who inspired me as a youth; my father, Paul Kushner, who inspires me to this day; and my partner, Beth Reimer, who might tolerate me into the future.

I would also like to thank my advisor, Dr. Feiyue Wang, for an endless number of things. Foremost for providing the foundation of this research and having the patience to see me through it. Secondly for showing me what it truly means to be an advisor and have a zeal for science. Lastly, for never passing up the opportunity to join me at the beginning of the earth.

I would like to thank the entire research group of Dr. Wang with a special mention to Deborah Armstrong and Heather Kyle. Debbie and I began our working relationship together at a hotel in Nicaragua. Our equipment was held up at customs with neither of us fluent in Spanish. She waited patiently for a week until it was released so I could go out exploring volcanoes. I probably had the better end of that arrangement.

From my committee I would like to thank Dr. Norman Halden who has shown me the importance of applying a geological background to problems outside of diorites and drill holes. I would also like to thank Dr. Peter Outridge for flying down to Winnipeg twice, both times in the winter, and for taking the time to edit my manuscript.

I would finally like to thank OVSICORI staff for time and arranging access during the field campaign. In particular Dr. Maarten de Moor, Dr. María Martínez, and Dr. Geoffroy Avard who all introduced me to the unexpectedly difficult concept of hiking into a volcano.

Table of Contents

List of Tables

List of Figures

List of Terms

Basalt: An extrusive igneous rock containing between 45 – 53 wt.% SiO_2

Andesite: An extrusive igneous rock containing between 52 – 63 wt.% SIO_2

Dacite: An extrusive igneous rock containing between 62 – 69 wt.% SIO_2

Rhyolite: An extrusive igneous rock containing > 69 wt.% SIO_2

Sub-Plinian Eruption: An explosive, gas-driven volcanic eruption with a plume height < 20 km

Phreatic Eruption: An explosion involving water or steam, driven by the rapid evaporation of cool water encountering heated magmatic products.

Phreatomagmatic eruption: A subcategory of phreatic eruptions involving the interaction of water with magma or lava. May also be termed as a surtseyan eruption.

List of Abbreviations

AAS: Atomic Absorption Spectroscopy

CAVA: Central American Volcanic Arc

COSPEC: Correlation Spectrometer

CVAFS: Cold Vapour Atomic Fluorescence Spectroscopy

DOAS: Differential Optical Absorption Spectroscopy

FTIR: Fourier Transform Infrared Spectroscopy

GEM: Gaseous Elemental Mercury

GOM: Gaseous Oxidized Mercury

MultiGAS: Multi-component Gas Analyzer

OVSICORI: Observatio Vulcanológico y Sismológico do Costa Rica

PBM: Particulate Bound Mercury

SINAC: Sistema Nacional de Areas de Conservacion

TAM: Total Atmospheric Mercury

UNA: Universidad National-Costa Rica

Chapter 1: Introduction

1.1 Objectives

To better understand the emissions and speciation of volcanic mercury (Hg), this study will carry out a comprehensive analysis of volcanic emissions over multiple phases of volcanic activity. Possible variations in emitted Hg concentrations may explain discrepancies between repeated measurements of the same volcano (e.g., Mt. Etna; Bagnato et al., 2014). Furthermore, measurements of Hg flux from a volcano over multiple stages of activity may better describe uncertainties related to volcanic emissions of Hg in a global context. Specifically, the objectives of my study are to:

1. Determine Hg concentrations in the air, soil, and water in the plume and along a distance gradient down plume of Poás volcano, Costa Rica.
2. Construct a new flux estimate for Poás volcano during the 2017 active period.
3. Extrapolate the changes in observed Hg/SO_2 ratios over multiple periods of activity to better constrain the global volcanic Hg inventory.

1.2 The global mercury cycle

1.2.1 Overview

Mercury is a toxic, non-essential metal considered by the World Health Organization (WHO) to be a major concern for human health (WHO, 2007). Inorganic forms of Hg are not readily bioaccumulated and are typically exposed to the average person over long times in low doses through inhalation of ambient gases, ingestion from foods, or exposure from dental and aesthetic products. Impaired kidney function is the most common adverse effect associated with inorganic Hg exposure, though there is an exhaustive list of other adverse effects (Park and Zheng, 2012). Under reducing conditions, bioavailable inorganic Hg may undergo biologically mediated reactions to organic methylated species, most notably by some sulphate- and iron-reducing bacteria

in anoxic waters and sediments (Fitzgerald and Lamborg, 2014). Organic forms of Hg readily bioaccumulate and are a recognised developmental neurotoxin to humans (WHO, 2007). Local contamination of Hg from industrial processes and discharge has led to abnormally elevated concentrations in communities such as Minamata, Japan and Grassy Narrows, Canada (Tsubaki and Irukayama, 1977; Wheatley and Paradis, 1995). Understanding Hg contamination is further complicated by the tendency of deposited Hg to volatilize into a gaseous elemental state, especially when heated to high temperatures or exposed to sunlight. Gaseous elemental Hg is less reactive than inorganic and organic Hg (II); this allows for long-range atmospheric transport to areas as remote as the high Arctic (Fitzgerald and Lamborg, 2014) and the Himalaya-Tibet region (Kang et al., 2016). As such, Hg is ubiquitous in the environment and all emissions represent a global, rather than local concern to humanity at large. Due to its global transport and negative impacts to both humans and animals, global efforts are underway to curb anthropogenic Hg emissions as mandated by the Minamata Convention on Hg (UNEP, 2013).

Anthropogenic activity has disturbed geologic Hg reservoirs, increasing the amount available in the environment. Trends of increased Hg deposition from the atmosphere are associated with higher atmospheric Hg concentrations. Depositional concentrations calculated from glaciers in North America (Schuster et al., 2002; Chellman et al., 2017), Asia (Kang et al., 2016), and the Arctic (Zheng, 2015) all demonstrate an increase in the global atmospheric Hg concentration over recent centuries. This increase is a direct result of anthropogenic emissions from industrialization, the main sources of which are coal fired power plants and artisanal small-scale gold mining, though other major sources include iron and cement production (AMAP/UNEP, in press). Debate still exists towards defining the specific time of overall anthropogenic perturbations of Hg in the environment. The onset of industrialization is often cited as a clearly

demarcated indicator (Chellman et al., 2017). Considering pre-industrial use of Hg in gold and silver mining, it has also been proposed (Outridge et al., 2018) that a more appropriate indicator for the onset of anthropogenic emissions may extend to the late 15th century. Atmospheric Hg concentrations and deposition patterns are not homogenously distributed (Lindqvist and Rohde, 1985; Prestbo and Gay, 2009; Pacyna et al., 2016) and some regions are not currently experiencing increasing atmospheric concentrations. Modern efforts to curb Hg emissions have produced decreasing trends in the amount recorded in middle-latitude North American ice and sediment cores. Projections by Pacyna et al. (2016) to 2035 show Hg emissions decreasing globally on the order of 0 to 35% under current policies, except for some localised increases, such as from China and India, where emissions are projected to increase by 0 to 60%. Best-case scenarios from the same study show global anthropogenic Hg emissions reduced by 35 to <60% from industrialised nations. Declining trends of anthropogenic emissions are driven by either a reduced dependence on fossil fuel energy or implemented regulations, such as scrubbing devices at coal power plants (Ma et al., 2017). Efforts to curb global Hg emissions have produced noticeable regional decreases in the amount of Hg deposited into the environment (Prestbo and Gay, 2009; Bael et al. 2015). This shows that practices curbing Hg emissions have favorable environmental responses within a sub-decade timespan.

Sources of atmospheric Hg may be subdivided into present day natural sources (volcanic, geogenic emission, etc. ; ~10%), present-day anthropogenic sources (coal burning, manufacturing, etc.; ~30%), and enviornmental processes which reemit previously deposited natural or anthropogenic Hg (ocean and soil evasion; ~60%) (AMAP/UNEP, in press). Present-day anthropogenic emissions were most recently assessed in 2015 at 2150 t a^{-1} (range 1960 – 2745 t a^{-1}), a 12% increase over previous assessments by the same reporting agency in 2010

(AMAP/UNEP, in press). The release of Hg to the atmosphere and oceans by subaerial and submarine volcanic processes is considered to be the major natural source of Hg, though disagreement exists over the global impact and the total quantity emitted (Pyle and Mather, 2003; Nriagu and Becker, 2003). Future climate change is anticipated to make available previously restricted deposits of Hg, adding additional reservoirs of natural Hg (e.g. Arctic permafrost; Schuster et al., 2018) that may be introduced into global flux calculations.

1.2.2 Volcanic emissions of mercury

It is well known that volcanoes are a primary natural source of Hg to the environment with the potential to either affect regional ecosystems through passive degassing or to dominate the global Hg budget through larger, explosive eruptions. Witt et al. (2008) have, for example, equated the Hg emissions of a Masaya volcano, Nicaragua, to the combined Hg emissions from coal and biomass burning in Central and South America. A modern day "Hg belt" of epithermal Hg-bearing deposits also closely follows active volcanic processes, suggesting that magmatic processes are involved in transporting Hg from crustal or mantle sources to these regions (Rytuba et al., 2003; Williams-Jones and Heinrich, 2005).

Past estimates of the volcanic contribution of Hg to the global background have ranged from very low (0.6 – 1.3 t a^{-1}; Ferrara et al., 2000) to very high (up to 1000 t a^{-1}; Nriagu, 1989), differing over three orders of magnitude. This large range is explained in part by limited datasets and the small number of volcanoes from which measurements have been made. More recent estimates suggested that the global Hg flux from volcanic sources is ~76 ± 30 t a^{-1} for passively degassing volcanoes (Bagnato et al., 2014) and an additional ~630 t a^{-1} for actively erupting volcanoes (Pyle and Mather, 2003). The more recent estimates were made under the assumption that explosive degassing carries a higher Hg/SO_2 ratio than passive degassing, and were also biased by infrequent, larger eruptions that only occurred a small number of times each century. This

estimation is evidenced by elevated Hg concentrations in ice cores for a small number of years coinciding with notable historic eruptions (e.g., Krakatoa and Mt. St. Helens; Chellman et al., 2017) or in sediment cores during increased times of volcanic activity (e.g., the K/T extinction event; Sanei et al., 2012). Fitzgerald and Lamborg (2014) suggested that inconsistencies remain regarding higher Hg/SO_2 ratios for erupting volcanoes, including the notable absence of the eruption of Mt. Pinatubo in 1991 from ice cores. It should also be noted that the 1912 Novarupta eruption, the largest of the 20^{th} century (Global Volcanism Program, 2013), is not recorded in the same ice cores that contain depositional Hg spikes attributed to eruptions of Mt. St. Helens and Krakatoa (Chellman et al, 2017). The uncertainty around Hg/SO2 ratios between different eruptive stages illustrates the need for additional measurements of Hg from eruption volcanoes.

1.3 Background information

1.3.1 Atmospheric speciation of mercury

Atmospheric Hg is typically grouped in three forms: gaseous elemental Hg (GEM), or Hg (0); gaseous oxidised Hg (GOM), which is primarily Hg (II) but may include some Hg (I) intermediates; and particulate-bound Hg (PBM) which is primarily Hg (II) but may contain some Hg(0). Typically, when considering the atmospheric concentrations, these forms are reported in abundance as total gaseous Hg (TGM) or total atmospheric Hg (TAM). TGM represents the sum of GEM and GOM while TAM represents the sum of GEM, GOM, and PBM (Driscoli et al., 2013). Each form has different properties affecting their abundance, depositional patterns, reactivity, and environmental impacts. Due to its chemical stability and low water solubility, GEM is the most abundant form of atmospheric Hg with the highest residence time (~3–6 months; Holmes et al., 2010; Horowitz et al., 2017). GOM and PBM are more reactive and/or water soluble than GEM and are subject to dry and wet scavenging to be deposited into soil or water systems. The higher water solubility of GOM leads to significantly shorter atmospheric residence times than

GEM (days to weeks), thus this species constitutes only a small percentage of total atmospheric Hg (Driscoli et al., 2013; Schroeder and Munthe, 1998). The large surface to volume ratio of atmospheric water droplets also provides an important medium for atmospheric scavenging and wet deposition of GEM and GOM or PBM, in addition to providing a medium for redox and complexation reactions to occur. After deposition, these forms may be subject to photo- or microbial-reduction and reemission.

The redox chemistry underpinning Hg atmospheric speciation remains plagued by uncertainties. Originally, the oxidation of GEM to GOM was thought to be a result of interaction between Hg and OH or O_3, and reduction of GOM to GEM was through H_2O in aqueous phase (Driscoli et al., 2013). Case studies from the Arctic have been seminal in resolving some uncertainties, including the role of halogens as a pathway for GEM oxidation to GOM. Schroeder et al. (1998) originally proposed a link between tropospheric depletion of GEM to depletion of O_3 during the first periods of sunlight in the Arctic. Subsequent work by Lindberg et al. (2002) further correlated rapid GEM depletion and GOM formation with the presence of halogens, specifically Br, in this environment. A summary of Hg pathways with gaseous and aqueous phase reactions and rate constants is available in Hynes et al. (2009), but atmospheric GEM chemistry pertinent to this research is simplified by Driscoli et al., (2013) as a two-step process:

$$Hg(0) + X + M \rightarrow HgX + M$$

$$HgX + Y + M \rightarrow HgXY + M$$

where X and Y can both be halogen radicals, while Y can also be another radical.

Considering the presence of GEM, halogens, heat, and water vapour in volcanic plumes, it is likely that that some oxidation of GEM to GOM will take place, allowing removal in the gas or vapour phase through wet or dry scavenging. This was modelled by von Glasow (2010) and Bagnato et al. (2013), where it was predicted that volcanic Hg originates from the vent as GEM

and is rapidly (> 90%) converted by halogens to PBM within five minutes after release. Validation of these models has been inconsistent and is not fully supported by field data. Speciated measurements using improvised devices similar in function to a Tekran 2537X (described in Witt et al., 2012) found that minutes after release from Masaya volcano, Nicaragua, GEM still made up >95% of TGM. These measurements were corroborated by work at Poás volcano by Bagnato et al. (2014). In contrast, Dedeurwaerder et al. (1982) found that a majority (>60 %) of the TGM from Mt. Etna was PBM.

1.3.2 Major volcanic gas emissions

Volcanic landforms emit large quantities of gas and ash over short periods during explosive eruptions. Between eruptions, volcanic gases are transported from an underlying reservoir to the atmosphere through fumaroles, geothermal fields, and soil diffusion. In cases such as Masaya, Etna, and Klyuchevskoy, volcanoes release tonnes to kilotonnes of gases between eruptive periods from a source in the caldera (Andres and Kasgnoc, 1998). This constant release of gas is known as persistent or quiescent degassing (Mather, 2015; Aiuppa, 2015). Explosive eruptions may eject material into a plume reaching above the troposphere, allowing for global transport of plume materials and short-term climate effects. Plume volatile materials typically originate as dissolved constituents in the source magma until an immiscibility point is reached. At the point of immiscibility, volatiles separate into singular or multi-phase gases, fluids, or supercritical fluids. Degassing primarily occurs depressurization through ascent of the magma into the crust rather than a result of cooling (Oppenheimer et al., 2014). Separated fluids originate as smaller immiscible bubbles or slugs that are less dense than the surrounding melt, causing an ascent to the surface. While travelling upwards, fluids begin to segregate into larger, fluid rich areas, building up more pressure on the overlying rock during ascent. These areas are inferred, using geophysical methods, to travel rapidly towards lower level reservoirs when a critical point of pressure buildup is reached,

leading to fracturing, followed by rapid movement towards the surface (Koulakov et al., 2012; Chiodini et al., 2016).

Volcanic gas emissions are spatially, temporally, and chemically heterogenous. Major constituents of volcanic plumes are variable in relative proportions, but generally consist of ~90% water (H_2O) followed by highly variable amounts of: sulfur species, mainly sulphur dioxide (SO_2) and hydrogen sulphide (H_2S); carbon species, mainly carbon dioxide (CO_2) and carbon monoxide (CO); and diatomic halogen gases in the form of chlorine (Cl_2), bromine (Br_2), and iodine (I_2). Ash, and other particulate matter will also be present (Aiuppa, 2015; Symonds et al., 1994). Minor volatiles that are emitted as gases but may quench to finer particles include trace concentrations of metals such as cadmium (Cd), selenium (Se), arsenic (As), and lead (Pb) (Symonds and Reed, 1993). The observed major inter-volcanic variability in major gas compositions may be related to source regions for volatile contribution, where different subducting oceanic slabs or mantle sources contain varying proportions of S, C, N, H, H_2O, and trace volatiles (Oppenheimer et al., 2014, Zimmer et al, 2008). Furthermore, incorporation of volatiles from wall rock and geochemical reactions in gas pockets during ascension may alter the chemistry and abundance of major gas species. Sulfur, for example, is typically expelled as SO_2 or H_2S, depending on the depth of the underlying hydrothermal system (Stix and de Moor, 2018). CO_2 has been isotopically determined to be strongly influenced by slab melting and crustal inputs in plume gases (Mason et al., 2017). Other common gases used to infer the magma source and degree of crustal contamination of volcanic sources are those that are depleted in the mantle and enriched in the crust, such as divalent nitrogen (N_2) and helium (He) (Zimmer et al., 3003).

The persistence and global ubiquity of passive degassing volcanic sources is important when considering global volcanic emissions. Time-averaged assessments from volcanic sources

suggest annual contributions of 13×10^6 t a^{-1} of emitted SO_2 from active eruptions (Andres and Kasgnoc, 1998) and 23×10^6 t a^{-1}, or 176 % of passive degassing (Carn and Fiolettov, 2017). The contribution of active eruptions is temporally inconsistent and typically dominated by a small number of eruptions each century (Global Volcanism Program, 2013). Disagreements exist over the exact global flux of some major and trace gases (Martin et al., 2010, 2012), but there exists a general confidence in volcanic SO_2 emission inventories, due in large part to the comparative ease of measurement and larger inventory of data (Andres and Kasgnoc, 1998, Oppenheimer et al., 2014)

Common methods for volcanic plume and gas analysis of materials are summarized in Mather et al. (2015), but generally consist of direct measurements and remote sensing techniques. Direct sampling of gases may take place using a device to directly collect gases in an evacuated chamber or into a solution into which the gases readily dissolve. The most common of these collection methods is the Giggenbach flask (Giggenbach, 1975). Particulate matter in the plume may also be collected onto filters (Martin et al., 2012) or collected afterwards as in settled ash layers. *In situ* measurements for major plume gases are also commonly made using a series of optical and electrochemical sensors bundled together into a multi-component gas analyser (MultiGAS) (see Aiuppa et al., 2005 for details) for analysis of CO_2, SO_2, and H_2S. Of additional note is the recent use of modulating sampling equipment for use on drones flown directly into the plume, thereby obtaining samples from previously difficult-to-access locations (Stix et al., 2018). Indirect measurements of major plume gases are used to produce total gas fluxes and are generally made using spectroscopic techniques. Variations include Differential Optical Absorption Spectrometers (DOAS), Fourier-Transform Infrared Spectrometers (FTIR), and Correlation Spectrometers (COSPEC or FLYSPEC). Instrumentation may be either mounted on the ground or

attached to a plane or satellites. Typically, an indirect spectrometry measurement is only used to acquire reliable fluxes for SO_2 emissions, as varying atmospheric background levels complicate the process of obtaining accurate CO_2 or H_2O fluxes, although some FTIR analysis has produced data on total major gas and halogen emissions (Oppenheimer and Kyle, 2008). Other measurements are then indexed to SO_2 emissions to obtain a total flux (Martin et al., 2012; Bagnato et al., 2014).

1.3.3 Techniques for quantifying volcanic gas emissions of mercury

Arguably the single most important contribution to uncertainties in the global volcanic Hg flux is the lack of available Hg measurements. Large databases of gas fluxes exist for major volcanic gases (e.g., SO_2, CO_2) at most volcanic observatories such as at Mt. Etna and Mauna Loa Volcano, where monitoring is constantly underway. These measurements are catalogued in publicly accessible databases such as the Global Volcanism Program (Global Volcanism Program, 2013) and have quantitative measurements dating back to the early 1960s. The study of Hg emissions, by contrast, is an area beset by temporal and spatial inconsistencies in data and methodologies (Nriagu and Becker, 2003; Mather and Pyle, 2004). The first measurements of volcanic Hg date back to the late 1970s and 1980s on several passively degassing volcanic fields such as Mt. St. Helens, Mauna Loa, and Mt. Etna (Unni et al., 1976; Ballantine et al., 1982; Varekamp and Buseck, 1986). These were followed by an expansion of studies in the late 1990s and early 2000s concentrating largely on European volcanoes (Ferarra et al., 2000; Aiuppa et al., 2007; Bagnato et al., 2007). Recent efforts have further expanded datasets by increasing the number of volcanoes studied, with a sampling frequency at each volcano ranging from as low as one sample in total (Gorely and Etna volcanoes; Bagnato et al., 2014) to more than 127 samples per day (Mt. Amiata; Cabassi et al., 2017). Sampling periods at plumes typically last between one and five days, though most studies tend to opt for sampling periods over the course of one day

(e.g., Bagnato et al., 2014). Most passively degassing volcanic sources have been the subject of only one plume-Hg study or, where no measurements of Hg were conducted, Hg concentrations were extrapolated from SO_2 data (Pyle and Mather, 2003; Nriagu and Becker, 2003). Studies in the past produced average Hg/SO_2 ratios that varied by orders of magnitude, with some workers attempting to separate passive and active degassing eruptions (Varekamp and Buseck, 1986; Nriagu and Becker, 2003), while others did not draw a distinction between eruptive types (Nriagu, 1989; Ferrara et al., 2000; Fitzgerald and Lamborg 2014). A compilation of past global flux assessments by Pyle and Mather (2003) suggested that the Hg/SO_2 mass ratio for flux estimations falls between $10^{-6} – 10^{-4}$ for passively degassing volcanoes and is higher for explosive eruptions. This estimate was later corroborated by a literature review and an extensive sampling campaign by Bagnato et al. (2011, 2014), in which 28 of 36 measured volcanoes were found to have ratios within the range proposed by Pyle and Mather (2003).

Analysis of volcanic gases for Hg concentration is typically performed with concurrent measurements of major gases using two complementary techniques in order to derive a total flux: a MultiGAS system and a DOAS system. These devices are widely used in the volcanic monitoring field (Bagnato et al., 2007, 2014; Witt et al., 2004; de Moor et al., 2016). Both systems analyze H_2O, CO_2, SO_2, and H_2S, which compose over 95% (in moles) of emitted volatiles (Shinohara, 2008). The paired gas/Hg mass ratios are then used to calculate total volcanic Hg flux. SO_2 is the most commonly indexed gas to Hg (Bagnato et al., 2011, 2014; Aiuppa et al., 2007; Witt et al., 2008; Ferrara et al., 2000), mainly because of the large size of the database for volcanic SO_2 measurements and greater consensus over the global volcanic SO_2 budget compared to other potential index gases such as CO_2 (Pyle and Mather, 2003). Some studies have included Hg/CO_2 ratios (Witt et al., 2008; Aiuppa et al., 2007) and Hg/H_2S ratios (Cabassi et al., 2017) for estimates.

In recent studies, analysis of Hg in the plume is increasingly carried out by means of gold trap collection followed by *in situ* or off-line analysis using either cold vapour atomic absorption spectrometry (CVAAS) or cold vapour atomic fluorescence spectrometry (CVAFS) (Witt et al., 2004; Bagnato et al., 2014; Castillo et al., 2011; Cabassi et al., 2017). *In situ* analysis is carried out using either a Lumex® (AAS) which contains an internal battery and may be transported directly to the plume, or a Tekran 2537A (CVAFS) which requires an external power source and is usually operated at a considerable distance down-plume. Samples collected using gold traps external to the analytical instrument such as the Tekran may also be analysed, *ex-situ* using CVAFS (Bagnato et al., 2014).

In volcanic environments, comparisons of Lumex® portable analyser and gold trap collection at-plume followed by CVAFS analysis off-site have shown mixed results. Aiuppa et al. (2005) and Bagnato et al. (2014) showed that Hg concentration values agreed to within ~15% between methods at Vulcano, Italy, and Turrialba Volcano, Costa Rica, respectively. In contrast, comparison of gold trap at plume to CVAFS techniques by Witt et al., (2008) has shown values 500% to 1900% higher using Lumex® instrumentation than gold traps at Masaya Volcano, Nicaragua. A possible explanation for disagreements between methods is high amounts of acidic gases (SO_X, NO_X, and halogen species) reacting with the gold traps, which could hinder Hg trapping efficiency, resulting in a low concentration bias (Witt et al., 2008).

1.4 Background geology of the study region

The Central American Volcanic Arc (CAVA) is the densest area of active volcanoes in the world (Figure 1.1; de Moor et al., 2016a). This volcanic belt was formed through subduction of the Cocos plate beneath the Central American plate (DeMets, 2001). A feature of this arc is the transition of dominant eruptive lithology from basaltic-andesitic in the north (e.g., Masaya and Momotombo volcanoes; Van Wyk de Vries, 1993) to dacitic-rhyolitic to the south (e.g., Poás and

Baru volcanoes; Prosser and Carr, 1987). The shift in eruptive lithology from North to South is assumed to be caused by the angle of Cocos plate subduction, which is steeper to the north (84° in Nicaragua) and gradually declines to the south (60° near Costa Rica and 30° around Panama; Pennington, 1981). The diversity of volcanism along the CAVA coupled with the presence of tourism infrastructure at most major volcanoes presents an opportunity to investigate variations in plume chemistry along the arc (Kutterolf et al., 2015; Aiuppa et al., 2014).

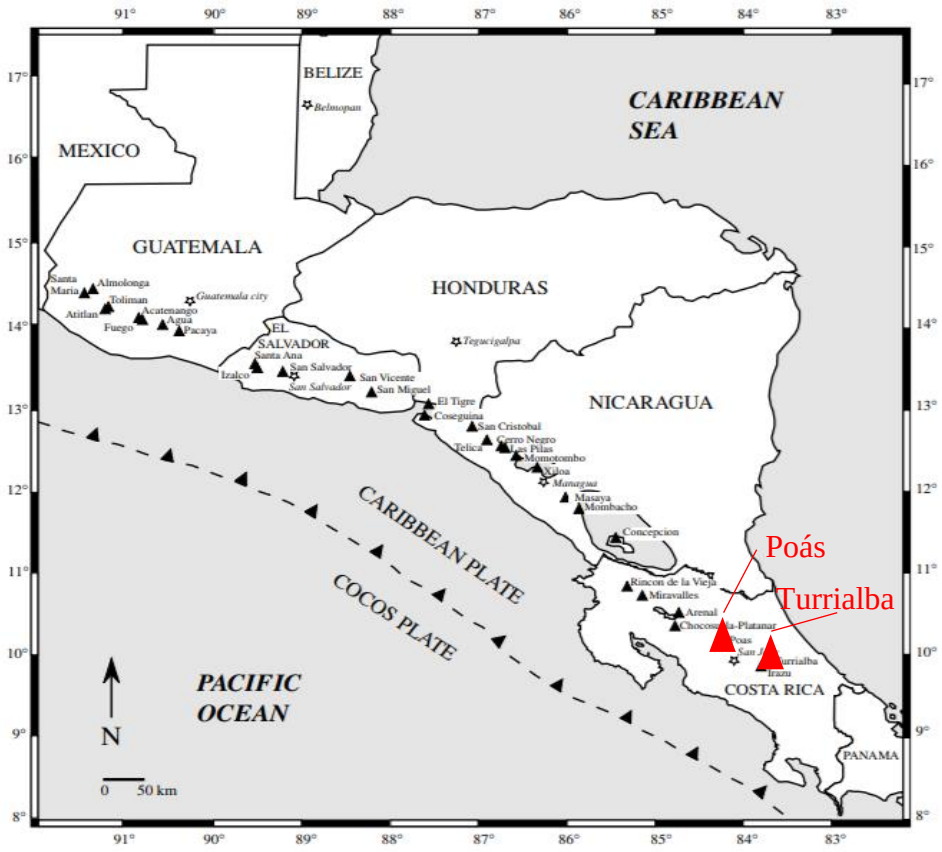

Figure 1.1: Plate interactions in Central America defining the CAVA and the location of active volcanoes along the arc (from Fischer, 2007). Poás and Turrialba volcanoes, studied in this thesis, are emphasised.

This research focuses on two active volcanoes within the CAVA, Poás and Turrialba. Turrialba (10.0163° N, 83.7649° W) is a basaltic-andesitic stratovolcano situated 3340 m above sea level. A marked increase in activity since 2010 has resulted in large passive emissions of ash and gases. In addition to passive degassing, six confirmed sub-Plinian eruptions have been reported

during this period reaching a plume height of 2 km and blanketing the capitol of San Jose in ash (Global Volcanism Program, 2013). Hydrothermal vents and pyroclastic cones are common from the base to caldera (Vaselli et al., 2010). SO_2 fluxes from the openly degassing vent at Turrialba are measured at between 590 t d^{-1} to 830 t d^{-1} during passive degassing (Xi et al., 2016) and >3000 t d^{-1} during eruptive periods (de Moor et al., 2016b).

Poás (10.1153° N, 84.1352° W) is a basaltic-andesitic stratovolcano situated 2708 m above sea level. Stratigraphy includes flow and pyroclastic sequences deposited from basaltic, andesitic, and dacitic magma sources (Ruiz et al., 2012; Prosser and Carr, 1987). This volcano undergoes daily to monthly phreatic eruptions from a hyper-acidic crater lake in the main crater (Martinez-Cruz, 2008; de Moor et al., 2016a) located next to a composite cinder cone (Ruiz et al., 2012). Eruptive phases typically occur every 10 – 20 years with the most recent period occurring in 2017. The eruptive period, lasting from May 2017 to September 2017, removed the overlying crater and adjacent lava dome lake, exposing a persistently degassing open vent and adjacent fumaroles. During the eruptive period, the SO_2 flux from Poás increased from < 10 t d^{-1} to 1944 t d^{-1} (de Moor et al., in press).

N_2/He, $\delta^{15}N$, and CO_2/S_T (total sulphur) analyses of volcanoes in the CAVA by Zimmer et al. (2014) suggested that Poás and Turrialba magmas are mantle derived with negligible amounts of slab contribution, and show that Turrialba has some crustal assimilation from shallow hydrothermal fluids. A mantle origin of these magmas was further corroborated by $\delta^{13}C$ analysis of condensates by Mason et al. (2017), showing mantle values for Poás and only a slight isotopic deviation caused by crustal contamination at Turrialba. The isotopic data acquired for these sites suggests that both magmas are more representative of the mantle and have assimilated less crustal materials then other subduction related volcanic sources where isotopic data has been gathered.

Recent studies of volcanic Hg emissions (Witt et al., 2008; Castillo et al., 2004; Bagnato et al., 2014) along the CAVA provided plume Hg concentrations and Hg/SO_2 ratios for several volcanoes (Table 1.1). Repeated measurements of GEM at Poás and Turrialba by Feiyue Wang (University of Manitoba, unpublished data), Castillo et al. (2011) and Bagnato et al. (2014) vary by two orders of magnitude. Poás and Rincón de la Vieja volcanoes also displayed anomalously low Hg/SO_2 ratios compared with similar volcanoes along-arc, leading to some of the lowest Hg flux estimates globally (Bagnato et al. 2014). To date, attempts to duplicate anomalously high results reported by Castillo et al., (2011) in urban environments (Haynes, 2012; Wang, unpublished data) and volcanic environments (Wang, unpublished data) have not been successful. Hence, conducting a thorough sampling program in a previously studied volcanic Hg source may be particularly important to assess the validity of the processes by which global volcanic Hg fluxes are estimated.

Table 1.1: GEM concentrations and GEM/SO_2 mass ratios from degassing sources in Costa Rica and Nicaragua. NR denotes a measurement which is not reported in the study.

Volcano	Reported GEM (ng m^{-3} ± sd. where given)	Reported GEM/SO_2	Study
Poás	6.0 ± 1.2	3.7×10^{-8}	Bagnato et al. (2014)
	583	NR	Castillo et al. (2011)
	1.23 ± 0.16	NR	Wang (Unpub. data)
Turrialba	81 ± 4	3.9×10^{-6}	Bagnato et al. (2014)
	57.4	NR	Castillo et al. (2011)
	1.05 ± 0.15	NR	Wang (Unpub. data)
Arenal	NR	6.0×10^{-4}	Ballentine et al. (1982)
Rincón de la Vieja	5.0 ± 0.6	3.5×10^{-6}	Bagnato et al. (2014)
Las Pailas	260	1.7×10^{-5}	Bagnato et al. (2014)
Las Hornillas	822	4.0×10^{-6}	Bagnato et al. (2014)
Masaya	163.5	2×10^{-5}	Witt et al. (2012)

1.5 References

Aiuppa, A. (2015): Volcano gas monitoring; Volcanism and Global Environmental Change; Schmidt, A., Fristad, K.E., and Elkins-Tanton, L.T. *Editors*; Pages 81-96.

Aiuppa, A., Bagnato, E., Witt, M.L.I., Mather, T.A., Parello, F., Pyle, D.M., and Martin, R.S. (2007): Real-time simultaneous detection of volcanic Hg and SO_2 at La Fossa Crater, Volcano (Aeolian Islands, Sicily); Geophysical Research Letters. Volume 34, 6 pages.

Aiuppa, A., Federico, C., Giudice, G., and Gurrieri, S. (2005): Chemical mapping of a fumarolic field: La Fossa Crater, Vulcano Island (Aeolian Islands, Italy); Geophysical Research Letters. Volume 32. Doi:10.1029/2005GL023207

AMAP/UNEP (in press): Technical Background Assessment for the 2018 Global Mercury Assessment; United Nations Environmental Programme: Geneva, Switzerland. 309 pages. <http://wedocs.unep.org/bitstream/handle/20.500.11822/21553/GMACombined.pdf?sequence=1&isAllowed=y>

Andres, R.J. and Kasgnoc, A.D. (1998): A time-averaged inventory of subaerial volcanic sulfur emissions; Journal of Geophysical Research; Volume 103, pages 25251-25261.

Bagnato, E. (2007) Estimates of Hg emission rates in active volcanic systems. Plinius Volume 33, pages 35–42.

Bagnato, E., Aiuppa, A., Parello, F., Allard, P., Shinohara, H., Liuzzo, M., Giudice, G. (2011): New clues on the contribution of Earth's volcanism to the global mercury cycle; Bulletin of Volcanology. Volume 73, pages 497-510.

Bagnato, E., Tamburello, G., Aiuppa, A., Sprovieri, M., Vougioukalakis, G.E., and Parks, M. (2013): Mercury emissions from soils and fumaroles of Nea Kameni volcanic centre, Santorini (Greece); Geochemical Journal. Volume 47, pages 437-450.

Bagnato, E., Tamburello, G., Avard, G., Martinez-Cruz, M., Enrico, M., Fu, X., Sprovieri, M., and Sonke, J.E. (2014): Mercury fluxes from volcanic and geothermal sources: an update; Geological Society of London, Special Publications. 24 pages.

Ballentine, D.S., Finnegan, D.L., Phelan, J.M., and Zoller, W.H. (1982): Measurement of Hg/S ratios from five volcanoes; EOS Transaction, American Geophysical Union. Volume 92, page 1152.

Beal, S.A., Osterberg, E.C., Zdanowicz, C.M., and Fischer, D.A. (2015): Ice Core Perspective on Mercury Pollution during the Past 600 Years; Environmental Science and Technology. Volume 49, pages 7641-7.

Cabassi, J., Tassi, F., Venturi, S., Calabrese, S., Capecchiacci, F., D'Alessandro, W., and Vaselli, O. (2017): A new approach for the measurement of gaseous elemental mercury (GEM) and H_2S from anthropogenic and natural sources: Examples from Mt. Amiata (Siena, Central Italy) and Solfatara Crater (Campi Flegrei, Southern Italy); Journal of Geochemical Exploration. Volume 175, pages 48-58.

Carn, S.A., Fioletov, V.E., McLinden, C.A., Li, C., and Krotkov, N.A. (2017): A decade of Global volcanic SO_2 measurements from space; Scientific reports; Volume 7, 12 pages.

Castillo, A., Valdes, J., Sibaja, J., Vega, I., Alfaro, R., Morales, J., Esquival, G., Barrantes, E., Paleah, B., and Lean, D. (2011): Seasonal and diel patterns of total gaseous mercury concentration in the atmosphere of the Central Valley of Costa Rica; Applied Geochemistry. Volume 26, pages 242-248.

Chellman, N., McConnell, J.R., Arienzo, M., Pederson, G.T., Aarons, S.M., and Csank, A. (2017): Reassessment of the Upper Fremont Glacier Ice-Core Chronologies by Synchronizing of Ice-Core-Water Isotopes to a Nearby Tree-Ring Chronology; Environmental Science and Technology. Volume 51, pages 4230-4238.

Chiodini, G., Paonita, A., Aiuppa, A., Costa, A., Caliro, S., De Martino, P., Acocella, V., and Vandemeulebrouck, J. (2016): Nature Communications. Volume 7, article number 13712, 9 pages.

Dedeurwaerder, H., Decadt, G., Baeyens, W. (1982): Estimations of mercury fluxes emitted by Mount Etna Volcano; Bulletin of Volcanology. Volume 45, pages 191-196.

DeMets, C. (2001): A new estimate for present-day Cocos-Carribean Plate motion: Implications for slip along the Central American Volcanic Arc; Geophysical Research Letters. Volume 28, pages 4043-4046

de Moor, J.M., Aiuppa, A., Pacheco, J., Avard, G., Kern, C., Liuzzo, M., Martinez, M., Guidice, G., and Fischer, T.P. (2016a): Short-period volcanic gas precursors to phreatic eruptions: insights from Poás Volcano, Costa Rica; Earth and Planetary Science Letters; Volume 442, pages 218-227.

de Moor, J.M., Aiuppa., A., Avard, G., Wehrmann, H., Dunbar, N., Muller, C., Tamburillo, G., Guidice, G., Moretti, R., Conde, V., and Galle, B. (2016b): Turmoil at Turrialba Volcano (Costa Rica): Degassing and eruptive processes inferred from high-frequency gas monitoring; Journal of Geophysical Research Solid Earth. Volume 121, pages 5761-5775.

Driscoli, C.D., Mason, R.P., Chan, H.M., Jacob, D.J., and Pirrone, N. (2013): Mercury as a global pollutant: Sources, Pathways, and Effects; Environmental Science and Technology. Volume 47, pages 4967-4983.

Ferrara, R., Mazzolai, B., Lanzillotta, E., Nocaro, E., and Pirrone, N. (2000): Volcanoes as emission sources of atmospheric mercury in the Mediterranian basin; The Science of the Total Environment. Volume 259, pages 115-121.

Fischer, T.P. (2007): Fluxes of volatiles (H_2O, CO_2, N_2, Cl, F) from arc volcanoes; Geochemical Journal. Volume 42, pages 21-38.

Fitzgerald, W.F. and Lamborg, C.H. (2014): Geochemistry of Mercury in the Environment, Chapter 11.4; Treatise on Geochemistry, 2nd edition. Editors: Heinrich Holland and Karl Turekian. Pages 91-129.

Global Volcanism Program (2013): Volcanoes of The World, v.4.7.0. Venzke, E (ed.); Smithsonian Institute; Downloaded 13 May, 2018. <http://dx.doi.org/10.5479/si.GVP.VOTW4-2013>

Giggenbach, W.F. (1975): A simple method for the collection and analysis of volcanic gas samples; Bullitin of Volcanology. Volume 39, pages 132-145.

Haynes, A.F. (2012): Mercury Contamination in Costa Rica; Honours thesis, Wesleyan University, U.S.A. < http://wesscholar.wesleyan.edu/etd_hon_theses/799/>

Holmes, C.D., Jacob, D.J., Corbitt, E.S., Mao, J., Yang, X., Talbot, R., and Slemr, F. (2010): Global atmospheric model for mercury including oxidation by bromine atoms; Atmospheric Chemistry and Physics. Volume 10, pages 12037-12057.

Horowitz, H.M., Jacob, D.J., Zhang, Y., Dibble, T.S., Slemr, F., Amos, H.M., Schmidt, J.A., Corbitt, E.S., Marais, E.L., and Sunderland, E.M. (2017): A new mechanism for anthropogenic mercury redox chemistry: implications for the global mercury budget; Atmospheric Chemistry and Physics. Volume 17, pages 6353-6371.

Hynes, A.J., Donohoue, D.L., Goodsite, M.E., and Hedgecock, I.M. (2009): Our current understanding of major chemical and physical processes affecting mercury dynamics in the atmosphere and at the air-water/terrestrial interfaces; Mercury Fate and Transport in the Global Atmosphere; Mason R., Pirrone N., Eds.; Springer: New York, 2009; pp 427–457.

Kang, S., Huang, J., Wang, F., Zhang, Q., Zhang, Y., Li, C., Wang, L., Chen, P., Sharma, C.M., Li, Q., Sillanpää, M., Hou, J., Xu, B., and Guo, J. (2015): Atmospheric Mercury Depositional Chronology |Reconstructed from Lake Sediments and Ice Core in the Himalayas and Tibetan Plateau; Environmental Science and Technology. Volume 50, pages 2859-2869.

Koulakov, I., Gordeev, E.I., Dobretsov, N.L., Vernikovsky, V.A., Senyukov, S., Jakovlev, A., and Jaxybulatov, K. (2012): Rapid changes in magma storage beneath the Klyuchevskoy group of volcanoes inferred from time-dependent seismic tomography; Journal of Volcanology and Geothermal Research. Volume 263, pages 75-91.

Kutterolf, S., Hansteen, T.H., Freundt, A., Wehrmann, H., Appel, K., Kruger, K., and Perez, W. (2015): Bromine and chlorine emissions from Plinian eruptions along the Central American Volcanic Arc: From source to atmosphere; Earth and Planetary Science Letters. Volume 429, pages 234-246.

Lindberg, S.E., Brooks, S., Lin, C.J., Scott, K.J., Landis, M.S., Stevens, R.K., Goodsite, M., and Richter, A. (2002): Dynamic oxidation of gaseous mercury in the Arctic troposphere at polar sunrise; Environmental Science and Technology. Volume 36, pages 1245 – 1256.

Lindqvist, O. and Rodhe, H. (1985): Atmospheric mercury–a review; Tellus. Volume 37B, pages 136-159.

Ma, Y.P., Mu, B.L., Yuan, D.L., Zhang, H.Z., Xu, H.M. (2017): Design of MnO2/CeO2-MnO2 hierarchical binary oxides for elemental mercury removal from coal-fired flue gas; Journal of Hazardous Materials. Volume 333, pages 186-193.

Martin, R.S., Mather, T.A., Pyle, D.M., Day, J.A., Witt, M.L.I., Hilto, R.G. (2010): Major and trace element distributions around active volcanic vents determined by analysis of grasses: implications for element cycling and bio-monitoring; Bulletin of Volcanology. Volume 72, pages 1009-1020.

Martin, R.S., Sawyer, G.M., Day, J.A., LeBlond, J.S., Ilyinskaya, E., and Oppenheimer, C. (2012): High-resolution size distributions and emission fluxes of trace elements from Masaya volcano, Nicaragua; Journal of Geophysical Research: Solid Earth. Volume 117, pages

Martinez-Cruz, M. (2008): Geochemical evolution of the acid crater lake of Poas volcano (Costa Rica): Insights into volcanic hydrothermal processes; Ph. D. Thesis, Utrecht University. 163 pages.

Mason, E., Edmonds, M., and Turchyn, A.V. (2017): Remobilization of crustal carbon may dominate volcanic arc emissions; Science. Volume 357, pages 290-294.

Mather T.A. (2015): Volcanoes and the environment: Lessons for understanding Earth's past and future from studies of present-day volcanic emissions; Journal of Volcanology and Geothermal research. Volume 304, pages 160-179.

Mather, T.A. and Pyle, D.M. (2004): Volcanic emissions of mercury to the total atmosphere: global and regional inventories, Comment; Science of the Total Environment. Volume 327, 323-329.

Mason, E., Edmonds, M., and Turchyn, V. (2017): Remobilization of crustal carbon may dominate volcanic arc emissions; Science. Volume 357, pages 290-294.

Miller, G.H., Giersdóttir, Á, Zhong, Y., Larson, D.J., Otto-Bliesner, B.L., Holland, M.M., Bailey, D.A., Refsnider, K.A., Lehman, S.J., Southon, J.R., Anderson, C., Björnsson, H., and Thordarson, T. (2012): Abrupt onset of the Little Ice Age triggered by volcanism and sustained by sea-ice/ocean feedback; Geophysical Research Letters; Volume 39, 5 pages.

Nriagu, J.O. (1989): A global assessment of natural sources of atmospheric trace metals; Nature. Volume 338, pages 47-49.

Nriagu, J. and Becker, C. (2003): Volcanic Emissions of Mercury to the Atmosphere: Global and Regional Inventories; Science of The Total Environment. Volume 304, pages 3-12.

Oppenheimer, C., Fischer, T.P., and Scaillet, B. (2014): Volcanic Degassing: Process and Impact; Treatise on Geochemistry (Second Edition). Volume 4, pages 111-179.

Oppenheimer, C. and Kyle, P.R. (2008): Probing the magma plumbing of Erebus volcano, Antarctica, by open-path FTIR spectroscopy of gas emissions; Journal of Volcanology and Geothermal Research. Volume 177, pages 743-754.

Outridge, P.M., Mason, R.P., Wang, F., Guerrero, S., and Heimburger, L-E. (2018): Updated global and oceanic mercury budgets for the United Nations Global Mercury Assessment 2018; Environmental Science and Technology. Volume 52, pages 11466-11477.

Pacyna, J.M., Travnikov, O., De Simone, F., Hedgecock, I.M., Sundseth, K., Pacyna, E.G., Steenhuisen, F., Pirrone, N., Munthe, J., and Kindbom, K. (2016): Current and Future Levels of Mercury Atmospheric Pollution on a Global Scale; Atmospheric and Chemistry Physics. Volume 16, pages 12495-12511.

Park, J.D. and Zheng, W. (2012): Human Exposure and Health Effects of Inorganic and Elemental Mercury; Journal of Preventative Medicine and Public Health; Volume 45, pages 344-352.

Pennington, W.D. (1981): Subduction of the Eastern Panama Basin and seismotectonics of northwestern South America; Journal of Geophysical Research, Solid Earth. Volume 86, pages 10753-10770.

Prestbo, E.M. and Gay, D.A. (2009): Wet deposition of mercury in the U.S. and Canada 1996-2005: Results and analysis of the NADP mercury deposition network (MDN); Atmospheric Environment. Volume 43, pages 4223-4233.

Prosser, J.T. and Carr, M.J. (1987): Poas volcano, Costa Rica: Geology of the summit region and spatial and temporal variations among the most recent lavas; Journal of Volcanology and Geothermal Research; Volume 33, pages 131-146.

Pyle, D.M. and Mather, T.A. (2003): The importance of volcanic emissions for the global atmospheric mercury cycle; Atmospheric Environment. Volume 37, pages 5115-5124.

Ruiz, P.R.C. (2012): Reconstruction of the paleo and neo stages of Poas and Turrialba Volcanoes, Costa Rica: competing processes of growth and destruction; Ph. D. Thesis, Rutgers University, 191 pages.

Rytuba, J.J. (2003): Mercury from mineral deposits and potential environmental impact; Environmental Geology; Volume 43, pages 326-338.

Sanei, H., Grasby, S.E., and Beauchamp, B. (2012): Latest Permian mercury anomalies; Geology. Volume 40, pages 63-66.

Schroeder, W.H., Anlauf, K.G., Barrie, L.A., Lu, J.Y., Steffen, A., Schneeberger, D.R., and Berg, T. (1998): Arctic springtime depletion of mercury; Nature. Volume 394, pages 331 – 332.

Schroeder, W.H. and Munthe, J. (1998): Atmospheric mercury- An overview; Atmospheric Environment. Volume 32, pages 809-822.

Schuster, P.F., Krabbenhoft, D.P., Naftz, D.L., Cecil, L.D., Olson, M.L., Dewild, J.F., Susong, D.D., Green, J.R., and Abbott, M.L. (2002): Atmospheric mercury deposition during the last 270 years: A glacial ice core record of natural and anthropogenic sources; Environmental Science and Technology. Volume 36, pages 2303–2310.

Schuster, P.F., Schaefer, K.M., Aiken, G.R., Antweiler, R.C., Dewild, J.F., Gryzeic, J.D., Gusmeroli, G., Hugelius, G., Jafarov, E., Krabbenhoft, D.P., Liu, L., Herman-Mercer, N., Mu, C., Roth, D.A., Schaefer, T., Striegl, R.G., Wickland, K.P., and Zhang, T. (2018): Permafrost Stores a Globally Significant Amount of Mercury; Geophysical Research Letters. Volume 45, pages 1463-1471.

Shinohara, H. (2008): Excess Degassing from Volcanoes and It's Role on Eruptive and Intrusive Activity; Review of Geophysics. Volume 45, 31 pages.

Sielgel, S.M. and Siegel B.Z. (1984) First estimate of annual mercury flux at the Kiluea main vent; Nature. Volume 309, pages 146-147.

Stix, J.J. and de Moor (2018): Understanding and forecasting phreatic eruptions driven by magmatic degassing; Earthm Planets and Space. Volume 70, 19 pages https://doi.org/10.1186/s40623-018-0855-z

Stix, J.J., de Moor, J.M., Rudiger, J., Alan, A., Corrales, E., D'Arcy, F., Diaz, J.A., and Liotta, M. (2018): Using Drones and Miniaturized Instrumentation to Study Degassing at Turrialba and Masaya Volcanoes, Central America; Journal of Geophysical Research: Solid Earth. Volume 123, pages 6501-6520.

Symonds, R.B. and Reed, M.H. (1993): Calculation of multicomponent chemical equilibria in gas-solid-liquid systems: Calculation methods. Thermochemical data, and application to studies of high-temperature volcanic gases with examples from Mt. St. Helens; American Journal of Science. Volume 293, pages 758-864

Symonds, R.B., Rose, W.I., Bluth, G.J.S., and Gerlach, T.M. (1994): Volcanic gas studies: methods,results and applications; Reviews in Mineralogy. Volume 1994, pages 1-60.

Tsubaki, T. and Irukayama, K. (1977): Minamata disease. Methylmercury poisoning in Minamata and Niigata, Japan; Tsubaki, T. and Irukayama, K. (eds.); North-Holland Publishing Company, P.O. Box 211, Amsterdam, The Netherlands; 317 pages.

UNEP. Global Mercury Assessment 2013 (2013): Sources, Emissions, Releases and Environmental Transport. United Nations Environment Programme Chemicals Branch, Geneva, Switzerland

Unni, C., Fitzgerald, W.F., Settle, D., Gill, G., Ray, B., Patterson, C.C. and Duce, R. (1978): The impact of volcanic emissions on the global atmospheric cycles of sulfur, mercury and lead; in Eos Transactions American Geophysical Union. Volume 59, page 1223.

Varekamp, J.C. and Buseck, P.R. (1986): Global Mercury Flux from Volcanic and Geothermal Sources; Applied Geochemistry. Volume 1, pages 65-73.

Wheatley, B. and Paradis, S. (1995): Exposure of Canadian Aborigional Peoples to Methylmercury; Mercury as a Global Pollutant. Pages 3-11.

Williams-Jones, A.E. and Heinrich, C.A. (2005): Vapor Transport of Metals and the Formation of Magmatic-Hydrothermal Ore Deposits; Economic Geology; Special Paper, Volume 100, pages 1287-1312.

Witt, M.L.I., Mather, T.A., Pyle, D.M., Aiuppa, A., Bagnato, E., and Tsanev, V.I. (2008): Mercury and Halogen Emissions from Masaya and Telica Volcanoes, Nicaragua; Journal of Geophysical Research Solid Earth. Volume 113, Issue B6, 15 pages.

World Health Organization (2007): Exposure to Mercury: A Major Public Health Concern; WHO Document Production Services, Geneva, Switzerland; 4 pages. <http://www.who.int/ipcs/features/mercury.pdf?ua=1>

van Wyk de Vries, B. (1993): Tectonics and magma evolution of Nicaraguan volcanic systems. PhD Thesis, Open University, Milton Keynes, UK.

Varekamp, J.C. and Buseck, P.R. (1986): Global Mercury Flux from Volcanic and Geothermal Sources; Applied Geochemistry. Volume 1, pages 65-73.

Vaselli, O., Tassi, F., Duarte, E., Fernandez, E., Poreda, R., Huertas, A.D. (2010): Evolution of fluid geochemistry at the Turrialba volcano (Costa Rica) from 1998to 2008; Bulletin of Volcanology. Volume 72, pages 397-410.

Von Glasow, R. (2010): Atmospheric Chemistry in Volcanic Plumes; Atmospheric Chemistry Special Feature. Volume 107, pages 6594-6599.

Zheng, J. (2015): Archives of total mercury reconstructed with ice and snow from Greenland and the Canadian High Arctic; Science of The Total Environment. Volume 509-510, pages 133-144.

Zimmer, M.M., Fischer, T.P., Hilton, D.R., Alvarado, G.E., Sharp, Z.D., and Walker, J.A., (2004): Nitrogen systematics and gas fluxes of subduction zones: Insights from Costa Rica arc volatiles; Geochemistry Geophysics Geosystems; Volume 5, 19 pages.

Chapter 2: Methods

2.1 Study Sites

For this research project, the study sites consisted of areas around two volcanoes along the Central American Volcanic Arc (CAVA) in Costa Rica: Poás volcano (10.1153° N, -84.1352° W; Figure 2.1), and Turrialba (10.0163° N, 83.7649° W; Figure 2.1). Two field campaigns were conducted from August to September, 2016, and from September to October, 2017. An additional dataset was provided by Dr. Feiyue Wang, consisting of *in situ* atmospheric Hg monitoring collected during 2015–2016 at Poás and Turrialba volcanoes. Field work for this research was carried out in collaboration with researchers from the Observatio Vulcanológico y Sismológico do Costa Rica (OVSICORI), a volcanic observatory associated with the Universidad National-Costa Rica (UNA).

2.1.1 Location and access

Poás and Turrialba volcanos were accessed with permission from, and in company of, OVSICORI personnel. A tourism industry around each volcano prior to eruptive periods has led to the development of roads to a lookout point, or "mirador", on the rim of both calderas. Traverses were made by foot from each mirador to sampling sites (Figures 2.2 and 2.3) using routes commonly used and deemed safe by OVSICORI personnel. Accessing Poás volcano during its active erupting stage (during the second field season) required additional permission from the Sistema Nacional de Areas de Conservacion Costa Rica (SINAC) for daily access to each park.

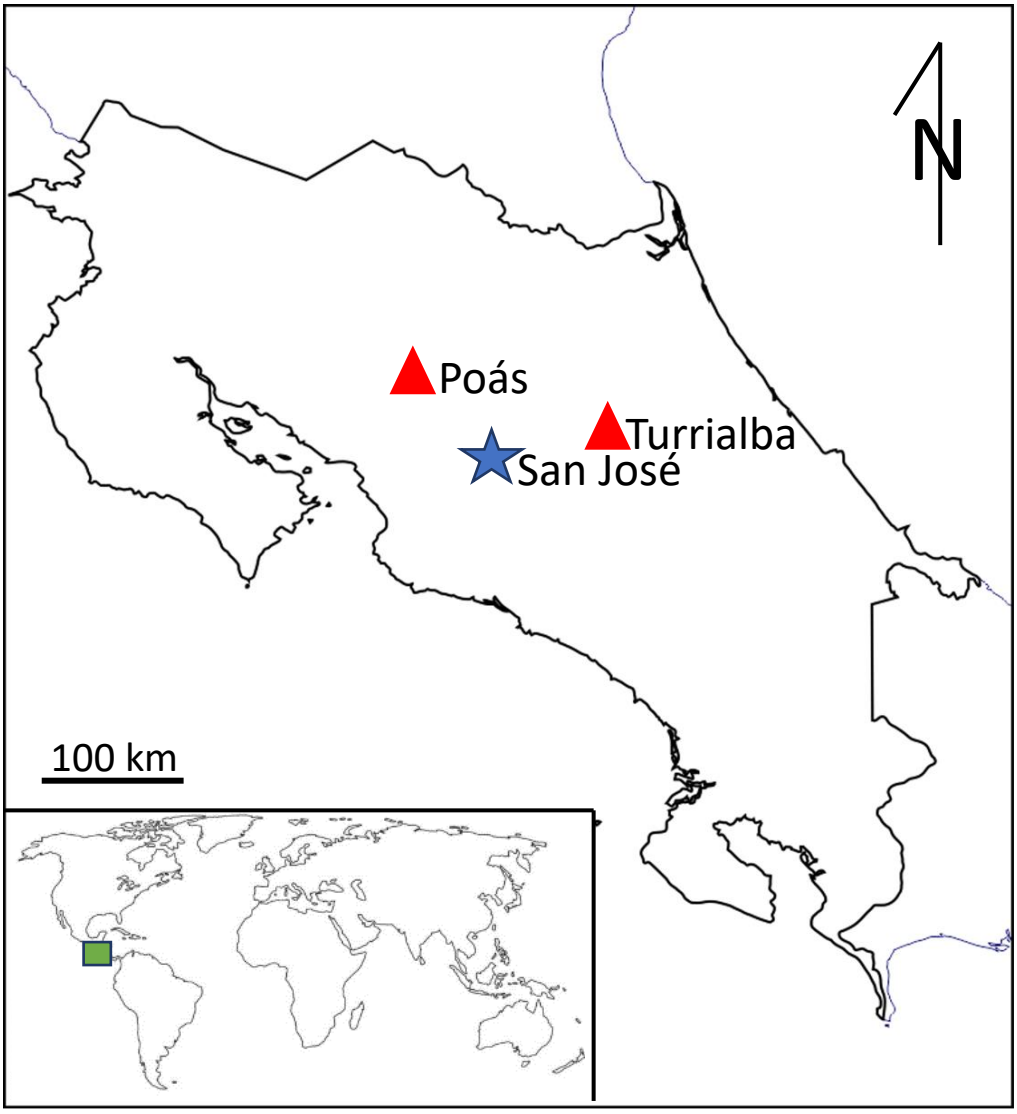

Figure 2.1: Location of Poás and Turrialba Volcanoes (red triangles) in Costa Rica relation to the capital city of San Jose (blue star).

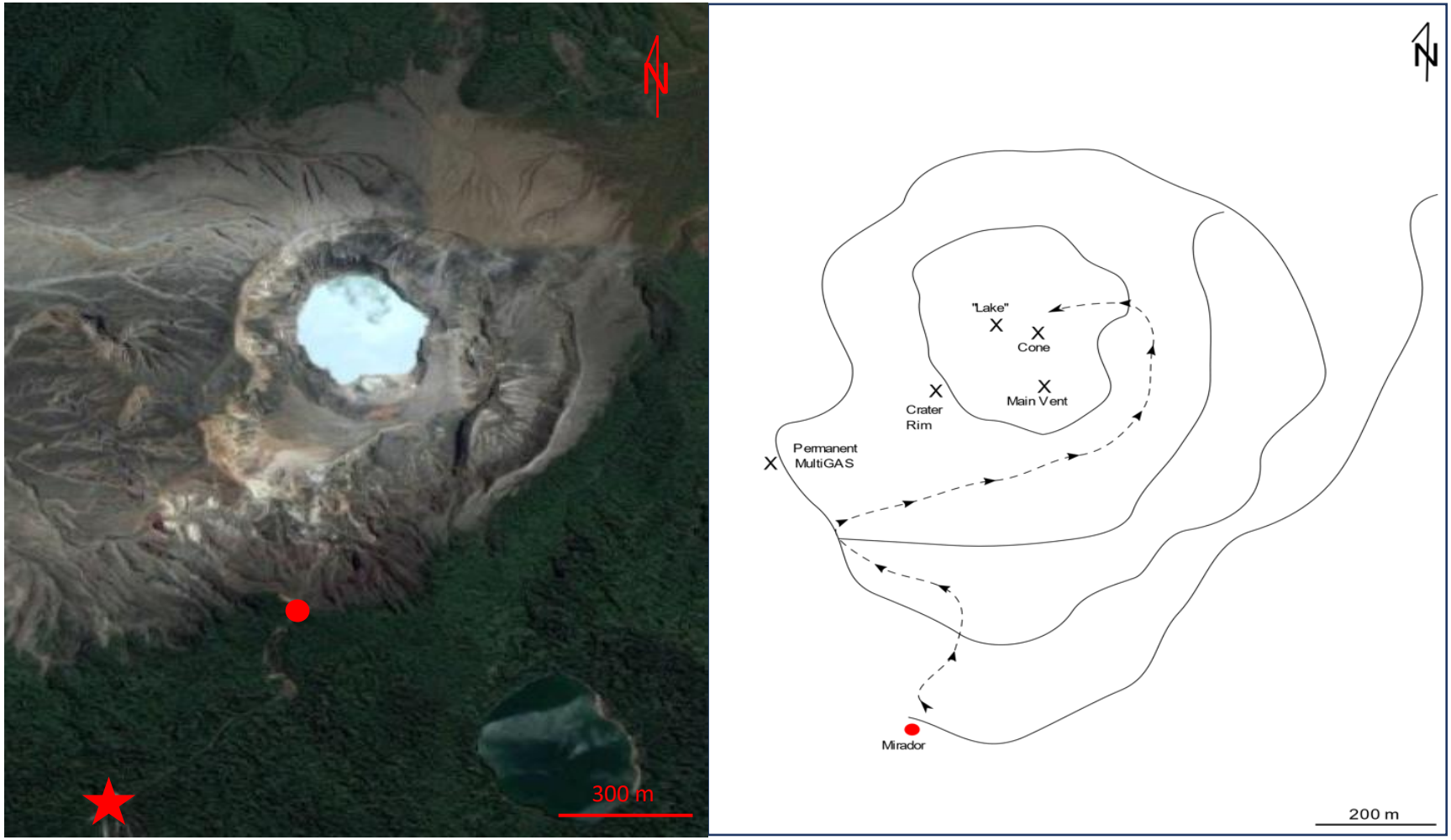

Figure 2.2: (left) Satellite image of Poás volcano including the locations of the mirador (red circle) and visitors centre (red star). (right) Trace of major topographic barriers for Poás including the locations of the mirador (red circle), individual sampling sites (black crosses), and general traverse route for access (dotted line).

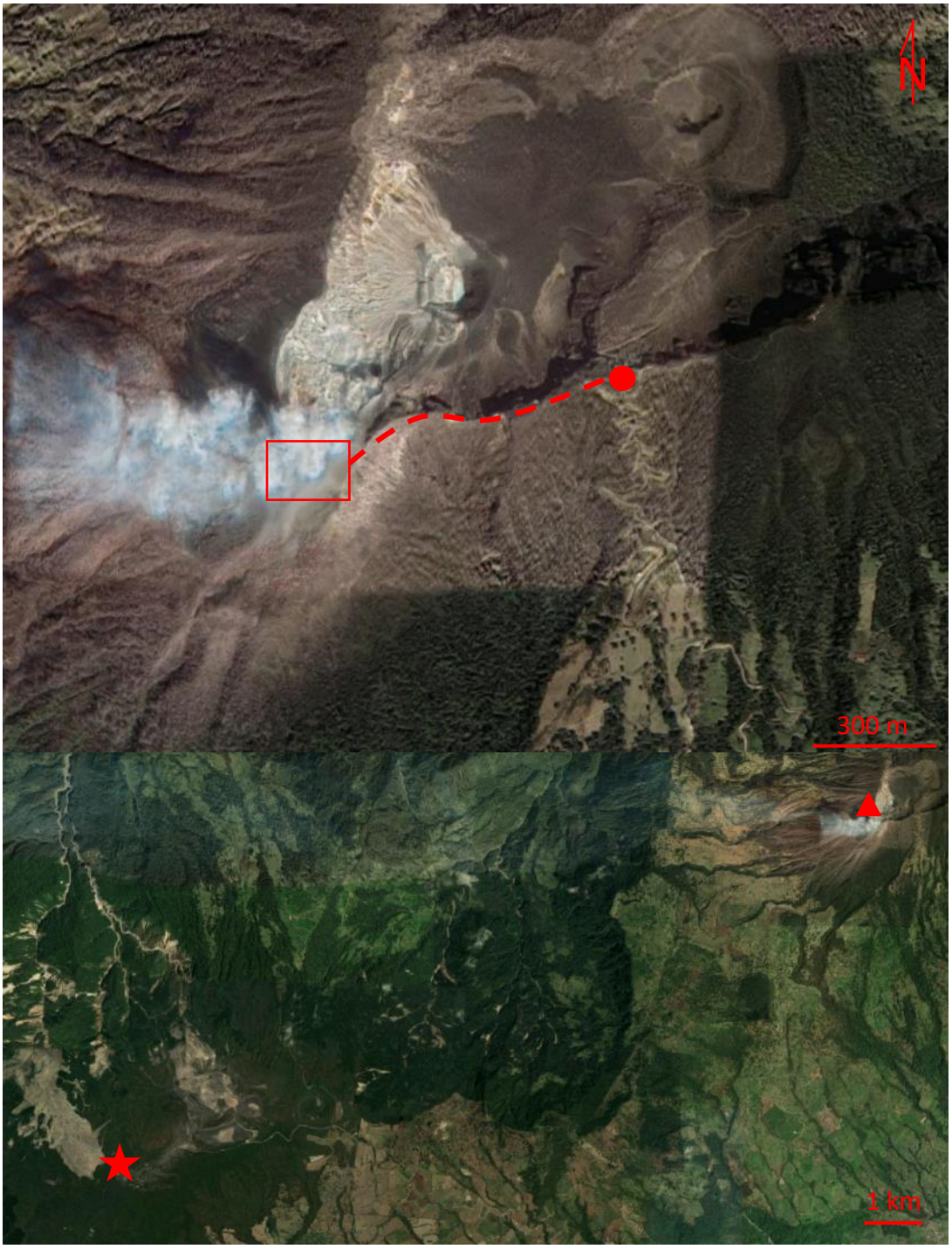

Figure 2.3: (top) Turrialba volcano indicating the mirador (red circle), traverse route (dashed red line), sampling area (red box), and hydrothermal vent (red triangle). (bottom) Enlarged view of surrounding Turrialba area indicating Turrialba volcano (top right) and long term atmospheric monitoring area (red star).

Site selection for atmospheric, ash, and water samples was determined based on safe access and maximized plume coverage (see Table 2.1 for full list of sampling locations). Ambient air samples were obtained from the mirador of each volcano. Monitoring stations for continuous atmospheric Hg sampling during 2015 by Dr. Feiyue Wang were chosen based on the requirement for a sufficient power supply. An additional suite of passive samplers was deployed at the same site in 2017 to assess annual variations (Figures 2.2 and 2.3).

Table 2.1: Detailed sample stations for 2015, 2016, and 2017 data collection.

Sampling Site	Sampling Station	Latitude (°N)	Longitude (°W)	Description	Sample Type	Date Sampled (dd/mm/yyyy)
Poás	Interpretative Centre	10.1855	84.2362	Used for 2015 continuous measurements and ambient passive sample collection	Continuous meas.	15/08/2015 – 25/01.2016 10/04/2016 – 14/04/2016
					Passive samplers	01/11/2017 – 24/11/2017
	Mirador	10.1904	84.2327	Used for 2017 ambient active sample collection	Active samplers	24/11/2017
	Lake	10.1976	84.2305	Used for 2016 water collection	Water	12/09/2016
	Main Vent	10.1965	84.2306	Location of measurements from Bagnato et al. (2014) in addition to both active and passive measurements in 2017	Active samplers	01/11/2017 – 24/11/2017
					Passive samplers	01/11/2017 – 24/11/2017
	Sulfur Cone	10.1976	84.2305	Cone ejecting elemental sulfur	Active samplers	01/11/2017 – 24/11/2017
					Passive samplers	01/11/2017 – 24/11/2017
					Ejecta	01/11/2017 – 24/11/2017
					Ash	01/11/2017 – 24/11/2017
	Borbollón	10.1974	84.2313	Liquid sulfur pool	Passive samplers	01/11/2017 – 24/11/2017
					Ash	01/11/2017 – 24/11/2017
					Ejecta	01/11/2017 – 24/11/2017
	Crater Rim	10.1961	84.2320	Rim of inner crater	Active samplers	01/11/2017 – 24/11/2017
					Passive samplers	01/11/2017 – 24/11/2017
					Ash	01/11/2017 – 24/11/2017
	Permanent MultiGAS	10.1952	84.2345	Rim of outer crater	Passive samplers	20/10/2017 – 01/11/2017
					Ash	01/11/2017

Turrialba	Ranger Station	9.9781	83.8340	Used for 2015 continuous measurements	Continuous meas.	01/02/2016 – 10/04/2016
	Tur-2016-01	10.0166	83.7656	Ash collection	Ash	08/09/2016
	Tur-2016-02	10.0189	83.7834	Ash collection	Ash	08/09/2016
	Tur-2016-03	10.0210	83.7628	Ash collection	Ash	08/09/2016

2.2 Sample collection and preparation

2.2.1 Atmospheric sampling

The first stage of sample collection for this project was initiated by Dr. Feiyue Wang during 2015. The measurements were taken using an automated Tekran system comprising model 1130 and 1135 speciation units with a Model 1102 air dryer and a 2537B Hg vapour analyser, following established procedures (Wang et al., 2014). The system was configured to measure GEM with a temporal resolution of 5 minutes, and GOM and PBM with a temporal resolution of 3 hours. All Hg data were recorded in units of ng m^{-3} or pg m^{-3} with the volume of air being corrected to standard conditions of 273 K and 1 atm (for reference 1 ppqv ≈ 8.9 pg m^{-3}). The detection limit (DL) was 0.1 ng m^{-3} for GEM and 0.4 pg m^{-3} for GOM and PBM. Calibration of the system was carried out daily with the built-in internal Hg permeation source in the Tekran 2537B detector, and monthly with manual injections of an external Hg source (Tekran Model 2505). It should be noted that while GEM and PBM measured by this technique provide a good estimate of Hg^0 and Hg bound to particles of diameters between ~0.1 – 2.5 μm, respectively, recent studies have shown that the KCl-coated denuder in the Tekran instrument does not efficiently collect all GOM compounds, and could underestimate GOM by up to several fold (Gustin et al., 2013; Huang et al., 2013). Therefore, GOM values reported in this study should be considered as the lower limits of GOM (Wang et al., 2014).

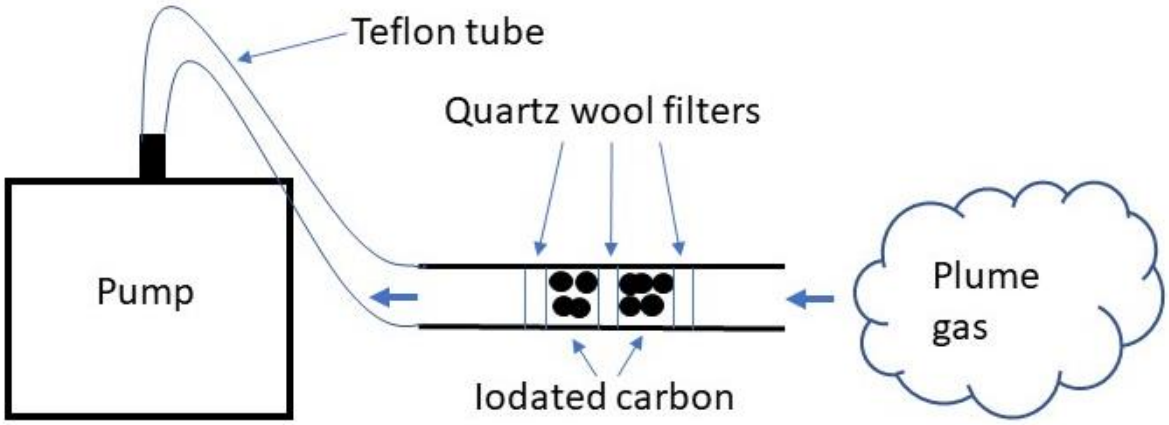

Figure 2.4: Schematic diagram of sampling setup used for active traps.

Two subsequent periods of atmospheric sample collection were conducted at Poás volcano (2016, 2017) and one at Turrialba volcano (2016). During the 2016 field season, active traps were collected using 3-mm diameter iodated carbon traps (Apex Instruments, part number MTB-U) attached to an Escort® ELF Air Sampling Pump (Sigma-Aldrich®, part number 28160-U) (Figure 2.4). Samples were collected from 40 min. to 3 h at a flow rate of 0.8 – 1.1 L min^{-1}. During the second field season, active traps were collected from Poás volcano using 10-mm diameter iodated carbon traps (Apex Instruments, part number MTB-U) attached to either an A.P. Buck Elite-1 pump (p.n. APB-908100) or the Escort® ELF Air Sampling Pump (Sigma-Aldrich®, p.n. 28160-U). Samples were collected from 3 – 2019 min at a flow rate of 1.28 – 2.6 L min^{-1}. Both the 3-mm and 10-mm traps contain two sections of iodated carbon separated by quartz wool. The rear section is intended as a field blank for detection of bleed-through and the quartz wool is used to trap particulate matter. Flow rates were determined using a calibrated flowmeter before and after every sample. The 10-mm traps were chosen over the 3-mm traps for the second period of sample collection, because a buildup of backpressure in the 3-mm traps was found to cause constant pump shutdowns resulting from flow rates outside of criteria (± 5%). The 3-mm traps were found to only support a maximum flow rate for sampling of

1.1 L min^{-1} while the 10-mm traps were found to be capable of supporting a consistent flowrate >3.0 L min^{-1}.

An alternate sampling arrangement was used at Poás for one station (crater rim) with the intention of long-term sampling. The design was constructed by connecting the A.P. Buck Elite-1 pump to an external 12 V battery using a 12 V to 6 V converter manufactured at the University of Manitoba; the setup was placed inside a waterproof Pelican™ case with outlets for air intake. 12-mm Teflon tubing was used to pump air from the outside at flow rates of 1.2 L min^{-1} for duplicate samples over periods of time ranging from 33 to 100 h.

Passive samplers were employed at each sampling site for Poás volcano during the active eruption stage. Samplers were constructed by the research group of Dr. Frank Wania at the University of Toronto (Figure 2.5). Each device consists of a sulfated carbon sorbent trap in a diffuse barrier, contained in a polypropylene casing with a removable lid for transportation to and from the field (further detailed and assessed within McLagan et al., 2017b; McLagan et al., 2015). Devices were zip-tied to a wooden stake at the same sampling sites as the active samplers in duplicate or triplicate for durations ranging from 7 to 21 days. Ambient conditions were assessed by placing duplicate sets of samplers at the visitors centre at heights of 2 m and 4 m. Field blanks were taken at each site visit by opening a blank sampler for ten seconds followed by sealing it up again. Travel blanks were left in the container used to transport the passive samplers from Winnipeg to Costa Rica. Flow rates for the passive samplers are determined to be 0.135 m^3 day^{-1} through comparative studies using Tekran instruments (McLagan et al., 2018). Shorter sampling periods were used for devices directly at the main vent due to concerns of corrosion from acidic gases in the plume destroying the inner stainless-steel mesh chamber (David McLagan, pers. comm.).

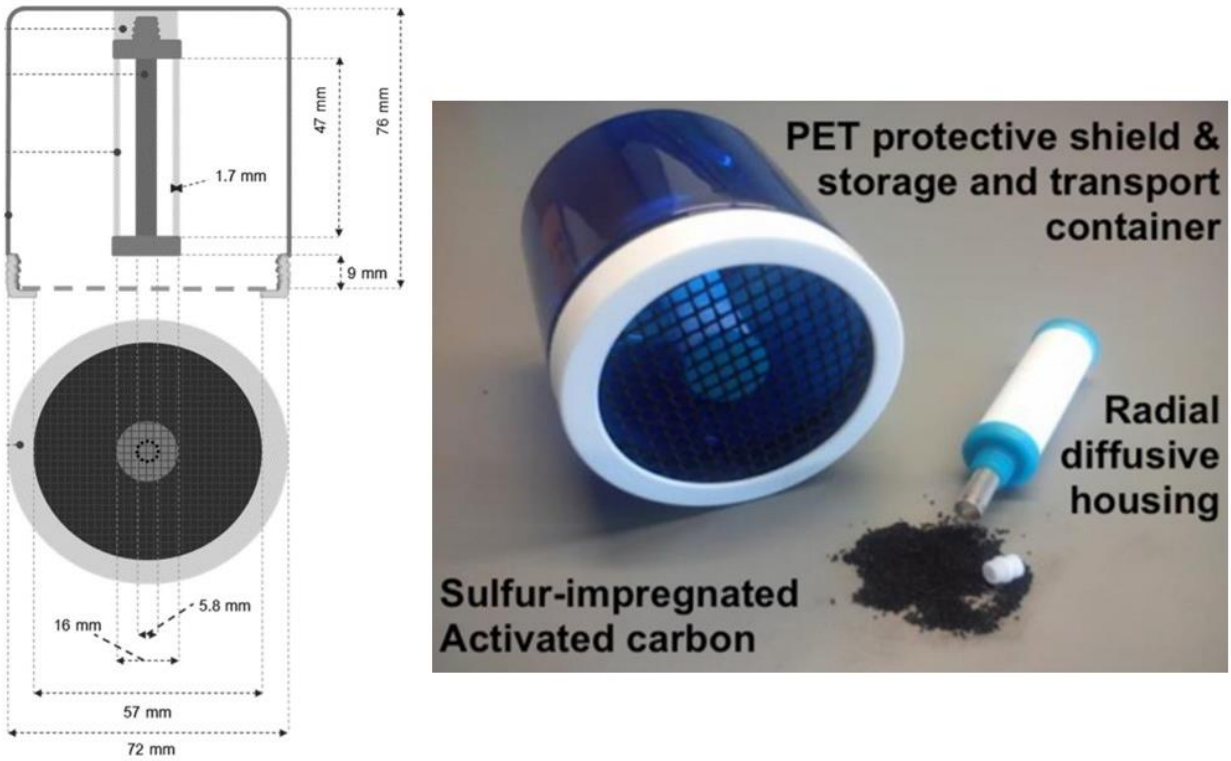

Figure 2.5: Schematic (left) and individual pieces (right) of the passive samplers used in this study (from McLagan et al., 2015).

To estimate an Hg/SO_2 ratio, simultaneous collection of major sulphur gaseous species (H_2S and SO_2) were taken using a 4 M NaOH solution within a bubbler (constructed by OVSICORI personnel). The bubbler used was essentially a variation of a Giggenbach flask (Giggenbach, 1975), and consisted of a pre-cleaned 500 ml graduated cylinder filled with ~100 ml of 4 M NaOH solution. The cylinder was closed with a rubber cork with two Teflon tubes fed through to different heights. One end was attached to a pump and another open to the atmosphere with a screen on the bottom. This allowed plume materials to be pumped and split into small bubbles, with both H_2S and SO_2 dissolved into solution. A flow rate of 1.0 L min^{-1} was measured from the bubbler using a flowmeter at site. Total sulphur species was collected using bubbler samplers and measured as total sulphate (SO_4^{2-}) by Ion Chromatography Mass Spectrometry (IC-MS) (data provided by Maria Martinez-Cruz, OVSICORI). Simultaneous monitoring from a permanent MultiGAS station

during the initial portions of the active phase of Poás measured an H_2S/SO_2 molar ratio of < 0.01 (de Moor et al., 2017) allowing for the approximation of SO_2 as the vast majority of all collected sulphur species.

2.2.2 Ash collection

Ash samples were collected at Turrialba in September 2016 and Poás in September 2016 and October – November 2017. Ash and plume materials were collected in 50 ml polypropylene tubes (Falcon®) from the top of passive samplers during the collection of each passive sampler from the field (Figure 2.6). This was used to provide a time constraint on the accumulated ash as deposited between the placement and removal of the passive sampler. Particulate matter collected on the glass wool filter in the iodated carbon traps was also separated. At each passive sampler for the 2017 sampling season, ash beneath the samplers was collected to test the possibility that there were localized spikes of Hg emitted from underlying hydrothermal systems (Lescinsky et al. 1987).

Figure 2.6: Ash buildup between sampling periods on Pelican case (left) and passive sampler (right).

2.2.3 Water collection

Water samples were collected from the edge of crater lake at Turrialba in September 2016 and from the edge of the crater lake at Poás in September 2016 and October – November 2017 (Figure 2.7). Collection vessels were new, 50-mL polypropylene vials (Falcon®) as part of a pre-constructed "field kit" following the *clean hands dirty hands protocol* (Fitzgerald, 1999). Each field kit was prepared at the Ultra-Clean Trace Elements Laboratory (UCTEL) at the University of Manitoba and consisted of two vials for duplicate sample collection and three vials dedicated for field blanks. As all the water samples were highly acidic (pH $\leq$ 1), no acid was added for preservation. The samples were shipped to the field and back to UCTEL with travel blanks to assess contamination during transport.

Figure 2.7: Sites of water sample collection: (top) Poás 2017, (bottom) Poás 2016

2.3 Sample analysis

2.3.1 Mercury analysis

Ash samples were freeze dried for 72 hours prior to analysis. Hg levels in ash, iodated carbon, and sulfated carbon were analyzed using atomic absorption spectroscopy (AAS) on a Hydra IIc Total Hg Analyser (Teledyne Leeman Labs) following the US EPA Method 7473 (USEPA, 1998). Samples were pyrolyzed in nickel boats with a drying stage of 300°C at 30 seconds and decomposition stage of 800°C for 120 seconds. Certified reference materials MESS-3, PACS-2, and Tort-2 (National Research Council of Canada) were used as external calibration standards and for QA/QC procedures (Table 2.2). The detection limit for analysis was 0.4 ng/g. Sodium carbonate was added to sample boats with sulfated carbon to prevent sulfur decay of the catalyst in the direct Hg analyser (as detailed in McLagan et al. 2017a).

Table 2.2: Certified value and range of certified reference materials compared to results from alanlysis

Certified Reference Material	Certified standard value [Hg_T] (ng g^{-1}) (accepted range)*	Analyzed average accuracy and standard deviation of [Hg_T] (ng g^{-1}) (n)
MESS-3	91 (82 – 100)	93 ± 4 (30)
PACS-2	3040 (2840 – 3240)	2918 ± 16 (30)
TORT-2	270 (210 – 330)	306 ± 15 (3)

*(National Research Council of Canada)

Water and collected ash samples on iodated filters were analysed for Hg using cold vapour atomic fluorescence spectroscopy (CVAFS) on a Tekran 2600 Hg Analyzer following U.S. EPA Method 1631 (U.S.EPA, 2002). 25 ml of undiluted sample were treated with 125 µl of BrCl, 125 µl of concentrated HCl, and 50 µl of hydroxylamine hydrochloride, in that order, before analysis. The detection limit was 0.2 ng L^{-1}.

AAS was chosen as the most suitable method for iodated traps as opposed to CVAFS, after difficulties were encountered with acceptable recoveries from iodated carbon traps during USEPA

method 30B digestion (USEPA 2009). These difficulties have been experienced with other labs (David McLagan, pers. comm.; Eric Prestbo, pers. comm.). CVAFS was chosen as the most suitable method for water samples due to the lower detection limits of the technique.

2.3.2 Materials characterization

Imaging of ash and collected materials was performed on a FEI Inspect S50 scanning electron microscope (SEM) with an attached Backscattered Electron (BSE) detector. Imaging was conducted under operating conditions of 20 kV and 15 nA.

2.4 Flux calculation and compilation of the literature on volcanic mercury

To calculate the Hg flux from Poás, the Hg concentrations in the plume were determined directly from the main vent from an active sampler. During the same time period, the plume SO_2 concentrations were determined ~30 cm away using a bubbler. The concentrations were then divided by the volume of plume sampled to determine a plume concentration per unit volume of air. The calculated plume-Hg concentration was then divided by the SO_2 concentrations to produce a Hg/SO_2 ratio for Poás. This ratio was then multiplied by the daily SO_2 flux from Poás for the total Hg emission per day. Due to non-ideal weather conditions during each visit to Poás, daily SO_2 fluxes are estimated and indexed to measurements published within de Moor et al. (in press). These fluxes are created using DOAS scans by OVSICORI personnel over the eruptive period. No flux was generated for Turrialba volcano due to lack of atmospheric Hg data for this site.

Atmospheric data for Poás were provided by Dr. Geoffroy Avard (pers. comm., UNA). Wind speed and wind direction were measured at hourly intervals over the sampling period. A wind rose constructed from these measurements was generated using MATLAB (R2013b).

To extrapolate towards a global Hg flux, data for comparison of volcanic Hg/SO_2 ratios were compiled from published studies. Eruptive frequency of examined volcanoes over the past 200 years have been compiled by the Global Volcanism Program database (2013). A plot of

eruptive frequency versus Hg/SO_2 was then constructed with a fitted curve using Sigmaplot (V.13.0). Only confirmed eruptions were considered for 200-year eruptive frequency. Hg/SO_2 data included for this series were collected preferentially using volcanic plume measurements, when available, to address discrepancies between main plume and fumarole measurements observed at other volcanoes (Witt et al., 2008; Pyle and Mather, 2013). Only direct gas measurements were included using a variety of chemical trap (e.g. Au traps) to account for discrepancies found in some studies using other instrumentation, such as those using filter packs (Kyle et al., 1990). An exponential decay equation was fitted to the data and used for the global flux estimation. Data for the 2006 – 2015 global flux estimate was compiled using the Global Volcanism Program Database (2013) by searching for all recorded eruptive events within the time period with no parameters (e.g., country, lower or upper threshold of SO_2 mass, altitude) excluded from the search. The eruptive frequency of each volcano identified as erupting during this time period was determined from the database, and the predicted Hg/SO_2 ratio was established using the equation of the fitted curve. The eruptive mass of SO_2 was combined with the predicted Hg/SO_2 ratio for each event to estimate an eruptive Hg mass. Total erupted Hg data for each year were grouped to provide an annual flux for each year between 2006 – 2015.

2.5 References

De Moor, J.M., Aiuppa, A., Avard, G., Diaz, J.A., Corrales, E., Rudiger, J., D'Arcy, F., Fischer, T.P., Stix, J., and Alan, A. (2017): A Sulfur Trigger for the 2017 Phreatomagmatic Eruption of Poas Volcano, Costa Rica? Insights from MultiGAS and Drone-based Gas Monitoring; American Geophysical Union. Fall Meeting 2017, abstract #V23F-04

Fitzgerald, W.F. (1999): Clean hands, dirty hands: Clair Patterson and the aquatic biogeochemistry of Hg; in Clean Hands: Clair Patterson's Crusade Against Environmental Lead Contamination; Davidson, C.I. ed.; Commack, NY: Nova Scientific Publishers, Inc. pages 119-137.

Giggenbach, W.F. (1975): A simple method for the collection and analysis of volcanic gas samples; Bullitin of Volcanology. Volume 39, pages 132-145.

Global Volcanism Program (2013): Volcanoes of The World, v.4.7.0. Venzke, E (ed.); Smithsonian Institute; Downloaded 13 May, 2018. <http://dx.doi.org/10.5479/si.GVP.VOTW4-2013>

Gustin, M.S., Huang, J., Miller, M.B., Peterson, C., Jaffe, D.A., Ambrose, J., Finley, B.D., Lyman, S.N., Call, K., Talbot, R., Feddersen, D., Mao, H., and Lindberg, S.E. (2013): Do We Understand What the Mercury Speciation Instruments Are Actually Measuring? Results of RAMIX; Environmental Science and Technology. Volume 13, pages 7295-7306.

Huang, J., Miller, M.B., Weiss, P., and Gustin, M.S. (2013): Comparison of Gaseous Oxidized Hg Measured by KCl-Coated Denuders, and Nylon and Cation Exchange Membranes; Environmental Science and Technology. Volume 47, 13 pages.

Kyle, P.R., Meeker, M., and Finnegan, D. (1990): Emission rates of sulfur dioxide, trace gases and metals from Mount Erebus, Antarctica; Geophysical Research Letters. Volume 17, pages 2125-2128.

Lescinsky, D.T., Connor, C., and Stoiber, R.E. (1987): Soil Mercury Study of Thermal Areas, Rincón de la Vieja Volcano, Costa Rica; Geothermics. Volume 16, pages 159-168.

McLagan, D.S., Mitchell, C.P.J., Huang, H., Lei, Y.D., Cole, A.S., Steffan, A., Hung, H., and Wania, F. (2015): A high-Precision Passive Air Sampler for Gaseous Mercury; Environmental Science and Technology Letters. Volume 3, pages 24-29.

McLagan, D.S., C.P.J. Mitchell, A. Steffen, H. Hung, C. Shin, G.W. Stupple, M.L. Olson, W.T. Luke, P. Kelley, D. Howard, G.C. Edwards, P.F. Nelson, H. Xiao, G.-R. Sheu, A. Dreyer, H. Huang, B. Abdul Hussain, Y.D. Lei, I. Tavchunsky, F. Wania. (2018): Global evaluation and calibration of a passive air sampler for gaseous mercury; Atmospheric Chemistry and Physics. Volume 18, pages 5905-5919.

McLagan, D.S., Huang, H., Lei, Y.D., and Mitchell, C.P.J. (2017a): Application of sodium carbonate prevents sulphur poisoning of catalysts in automated total mercury analysis; Spectrochimica Acta Part B: Atomic Spectroscopy. Volume 133, pages 60-62.

McLagan, D.S., Mitchell, C.P.J., Huang, H., and Wania, F. (2017b): The effects of meteorological parameters and diffuse barrier reuse on the sampling rate of a passive air sampler for gaseous mercury; Atmospheric Measurement Techniques Discussions. 22 pages. <https://www.researchgate.net/publication/316633474_The_effects_of_meteorological_parameters_and_diffusive_barrier_reuse_on_the_sampling_rate_of_a_passive_air_sampler_for_gaseous_mercury>

Pyle, D.M. and Mather, T.A. (2003): The importance of volcanic emissions for the global atmospheric mercury cycle; Atmospheric Environment. Volume 37, pages 5115-5124.

USEPA (1998): Method 7473 (SW-846): Mercury in Solids and Solutions by Thermal Decomposition, Amalgamation, and Atomic Absorption Spectrophotometry. 17 pages. <https://www.epa.gov/sites/production/files/2015-07/documents/epa-7473.pdf>

USEPA (2002): Method 1631, Revision E: Hg in water by oxidation, purge and trap, and cold vapor atomic fluorescence spectrometry; US Environmental Protection Agency. Washington, DC. 45 pages. <https://www.epa.gov/sites/production/files/2015-08/documents/method_1631e_2002.pdf>

USEPA (2009): Method 30B, Determination of Total Vapour Phase Mercury Emissions from Coal-Fired Combustion Sources Using Carbon Sorbent Traps; US Environmental Protection Agency. Washington, DC. 23 pages. < https://www3.epa.gov/ttnemc01/promgate/Meth30B.pdf>

Wang, F., Saiz-López, A., Mahajan, A.S., Gomez Martin, J.C., Armstrong, D., Lemes, M., Hay, T., and Prados-Roman, C. (2014): Enhanced production of oxidised mercury over the tropical Pacific Ocean: a key missing oxidation pathway; Atmospheric Chemistry and Physics. Volume 14, pages 1323-1335.

Witt, M.L.I., Mather, T.A., Pyle, D.M., Aiuppa, A., Bagnato, E., and Tsanev, V.I. (2008): Mercury and Halogen Emissions from Masaya and Telica Volcanoes, Nicaragua; Journal of Geophysical Research Solid Earth. Volume 113, Issue B6, 15 pages.

Chapter 3: Results

3.1 Mercury concentrations in water and ash samples

Mercury concentrations in the crater lakes were measured sporadically during the study period, and the results are shown in Table 3.1. Hg concentrations in the surface waters of the crater lake at Poás volcano during the 2016 sampling event were 6.4 – 8.7 ng L^{-1} (n=2); the temperature was 56°C during the sampling time. For the 2017 active period, Hg concentrations were between 0.8 – 1.6 ng L^{-1} (n=4) in a vigorously bubbling hydrothermal pool (t = 67°C). The meteoric-fed crater lake at Turrialba volcano was visited only during the 2016 season and had a Hg concentration of 72.5 g L^{-1} (n=1) in the surface water. Both water bodies had high amounts of turbidity when sampling, suggesting a large amount of suspended particulate matter.

Table 3.1: Mercury concentrations in the surface water of crater lakes (ND indicates no data)

Volcano	Site	Sampling date (dd/mm/yyyy)	Temperature (°C)	$[Hg_T]$ (ng L^{-1}) (mean ± sd; n)
Poas	Crater lake	12/09/2016	56	7.6 ± 1.2 ng L^{-1} (n=2)
	hydrothermal feature	17/11/2017	67	1.2 ± 0.4 ng L^{-1} (n=4)
Turrialba	Crater lake	09/09/2016	ND	72.5 g L^{-1} (n=1)

Mercury concentrations in ash collected from Poás during the 2017 active phase increased along a sampling transect (Sites A, D, E; Figure 3.1) from 4.4 – 5.4 ng g^{-1} (n=2) at the main vent to 17.9 – 19.9 ng g^{-1} (n=2) furthest down plume. A point of ~200 m from the main vent (Site D; Figure 3.1) had an ash Hg concentration of 13.3 ng g^{-1} (n=1), ~10% the concentration of ash collected from a similar distance from the main vent at Turrialba of 160.0 ng g^{-1} (Table 3.2). The highest measured ash concentration from Poás was 165.6 ng g^{-1} (n=1) taken directly from the borbollón (Station C, Figure 3.1) and areas immediately surrounding it.

Table 3.2: Mercury concentrations from ash samples collected from passive samplers (ND indicates no data)

Volcano	Sampling site (Letter on figure 3.1)	Approx. distance from source (m)	Sampling date (dd/mm/yyyy)	$[Hg_T]$ (ng g^{-1}) (mean ± sd; n)
Poás	Main Vent (A)	0	10/11/2017, 24/11/2017	4.8 ± 0.5 (2)
	Sulphur Cone (B)	5	24/11/2017	14.6 (1)
	Borbollón (C)	5	17/11/2017	165.6 (1)
	Crater Rim (D)	200	01/11/2017	13.3 (1)
	Permanent MultiGAS (E)	400	20/10/2017, 01/11/2017	18.5 ± 0.5 (2)
	Interoperative Center (X)	1200	ND	ND
Turrialba	Main Vent	200	08/09/2016	160.0

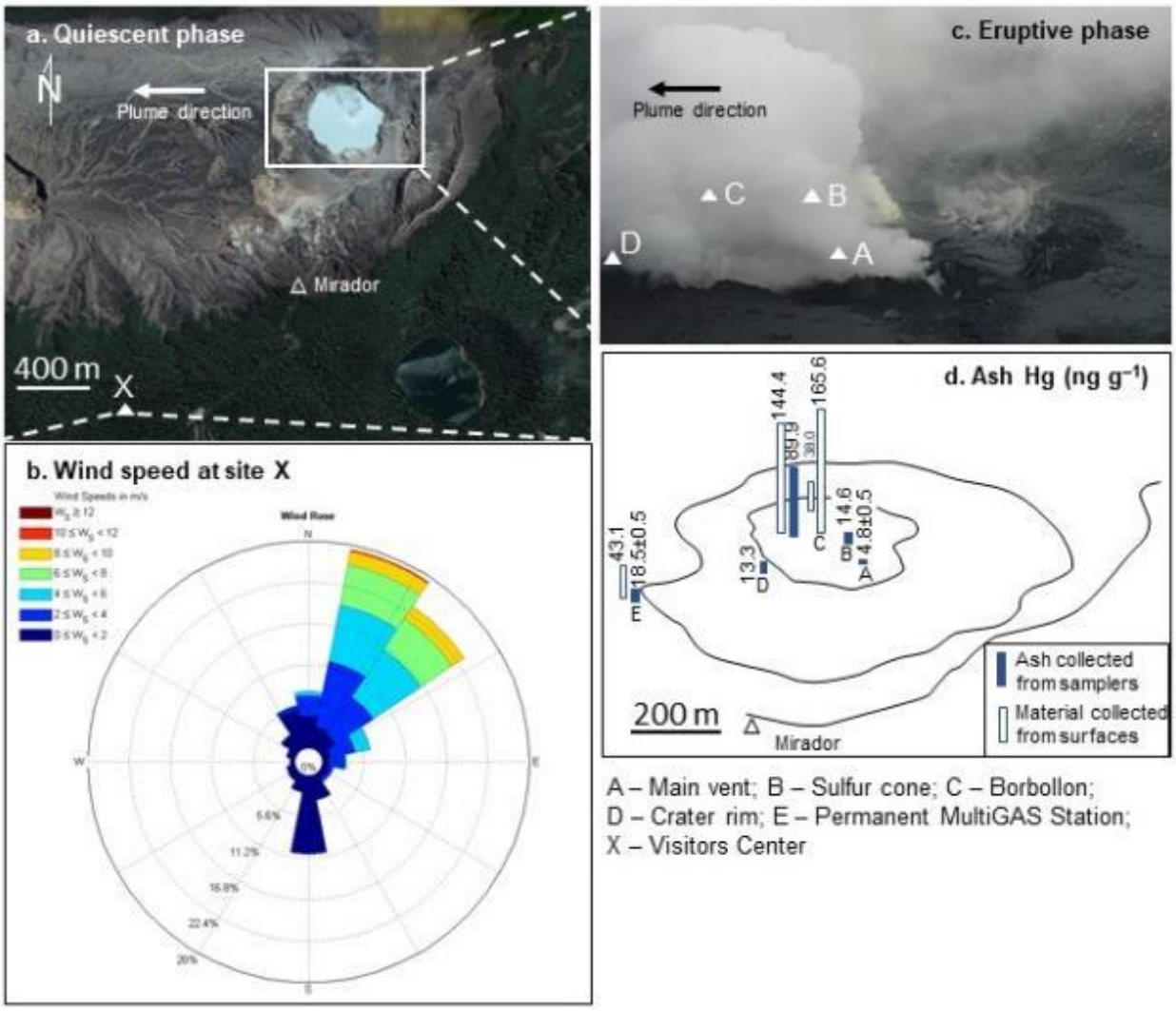

Figure 3.1: Poás Volcano during the quiescent (a) and active (c) phases. Panel (b) shows hourly wind direction and speed over the sampling period. Panel (d) shows Hg concentration in ash at each sampling site within Poás during the active phase of 2017.

The highest measured Hg concentrations in solid materials (ash or rock) from Poás was analysed in solidified material collected directly from the borbollón (Station C, Figure 3.1). Ash samples from the area immediately surrounding the borbollón also had a higher Hg concentration than ash collected from the main vent or cinder cone. To better understand why the borbollón was elevated in Hg, samples from features on the crater floor (A, B, and C; Figure 3.1) were imaged and analysed using SEM/EDX (Figure 3.2). The borbollón was found to be composed of ~60% euhedral elemental sulphur microliths, ~35% amorphous iron sulphide (observed as liquid at the

time of sample collection and solidified immediately after removal from the borbollón), ~5% subhedral accessory silicates including epidote and pyroxenes. Images of ash samples near the borbollón show a high portion of small particles ejected from this feature in addition to ash from the main vent. Imaging of material from the sulphur cone shows a composition of almost entirely (>95%) elemental sulphur with accessory gypsum occurring along fractures and within cavities (Figure 3.2).

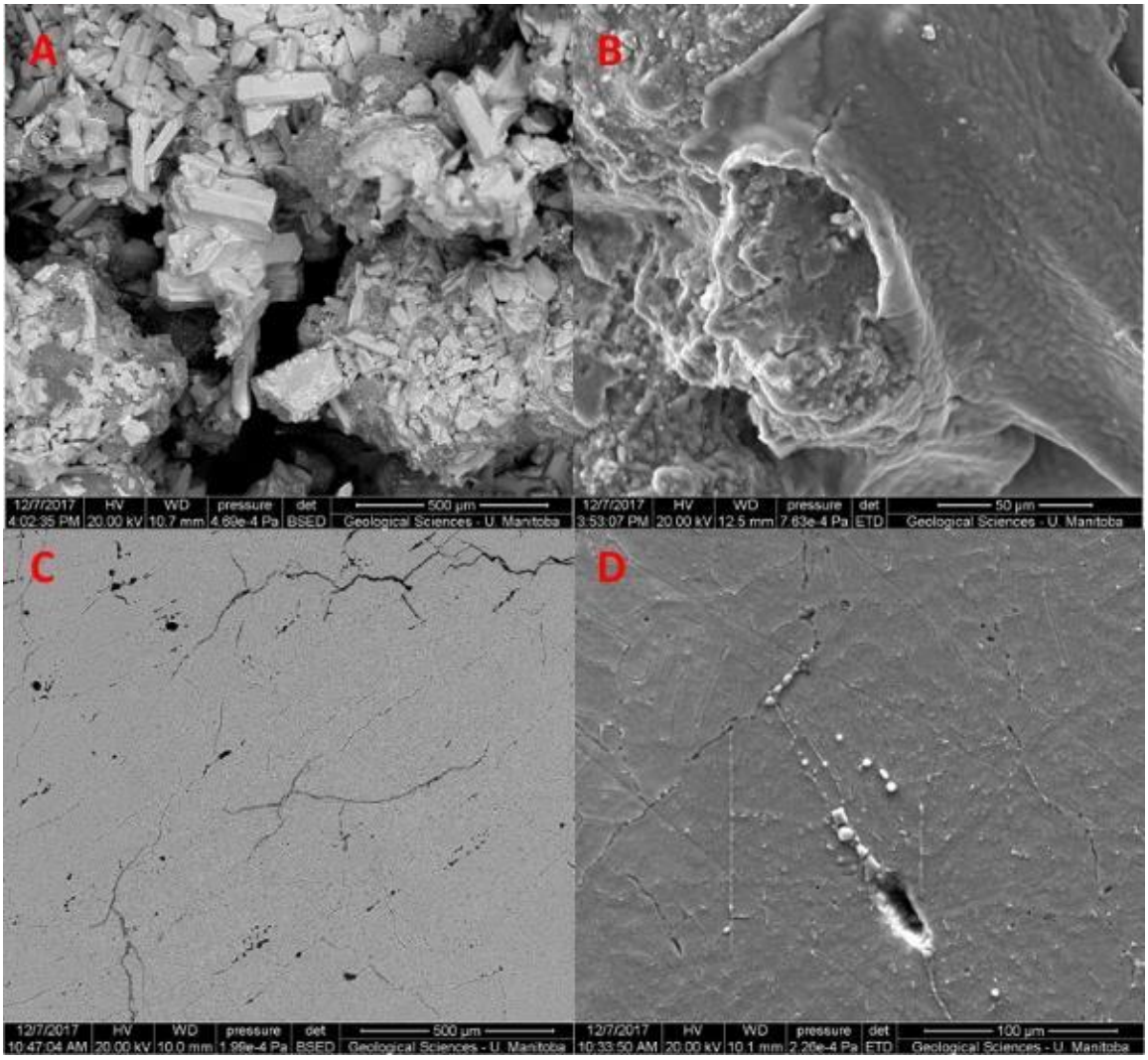

Figure 3.2: A) Back-scattered electron (BSE) image of collected material from the borbollón showing microliths of native sulphur (lighter grey); B) Scanning electron microscope (SEM) image of amorphous iron sulphide covering elemental sulphur; C) BSE image of elemental sulphur ejected from the sulphur cone showing homogenous composition and lack of internal structure; D) SEM image of sulphur from sulphur cone showing mineralization of gypsum (white to light grey) between fractures.

3.2 Mercury concentrations in volcanic emissions

During the inactive phase of Poás, atmospheric GEM was measured at the interpretative center (station X, Figure 3.3) to be 1.23 ± 0.16 ng m^{-3} (range: 0.61–3.73 ng m^{-3}; n = 43,375 over 5 months at a resolution of 5 minutes). Speciated measurements for GOM and PBM taken during the final period of sampling at Poás showed their concentrations were very low (< 4 pg m^{-3}), less than 1% of GEM. During the same sampling campaign, atmospheric Hg was measured down plume from Turrialba volcano to be 1.05 ± 0.15 ng m^{-3} (range: 0.47 – 3.46 ng m^{-3}; n = 11,063 over 2 months at a resolution of 5 minutes).

During the active phase of Poás, atmospheric samples collected along the transect (stations A, D, E; Figure 3.3) from the volcano were highest in Hg concentration at the main vent (2.4 – 16.8 ng m^{-3}; n=8) and declined at the crater rim (1.9 – 3.9 ng m^{-3}; n=11) and permanent MultiGAS station (3..7 – 3.9 ng m^{-3}; n=2). The lowest Hg concentrations on the crater floor were from the borbollón (2.1 – 4.9 ng m^{-3}; n=5) and the highest were from the sulphur cone (8.9 – 24.2 ng m^{-3}; n=5). An active sampler used to collect air at the mirador determined Hg concentrations of 1.2 ng m^{-3} (n=1). Passive samplers set up over the entire field campaign at heights above ground of 2 m and 4 m had Hg concentrations of 1.2 ± 0.0 ng m^{-3} (n=2) at 2 m and 1.2 (n=1) at 4 m. A full list of concentrations and the volume of atmosphere collected for each passive and active sampler is shown in Appendix 1.

A 2-way analysis of variance (ANOVA) test was performed on the data from active and passive samplers at the crater rim station (D, Figure 3.3). It is difficult to directly compare the two methods because the two sampling methods collect samples over different sampling durations (hours for active samplers and days for passive samplers) (Table 3.3). However, due to a single active sampler collecting over a prolonged period (33 hours), the test was performed to compare the factors of time duration (hours vs. days) and method (active vs. passive). The results showed

that there is not a statistically significant difference in measurement over time duration ($p = 0.989$) or over sampling method ($p = 0.691$). Therefore, the data from both the passive and active samplers are pooled together for the purposes of discussion and graphical representation (Figure 3.3).

To assess TAM, the proportion of GEM to PBM was analyzed from an active sampler at station D (Figure 3.3). Average wind speed during the sampling duration at this site was 2.6 m s^{-1}, allowing for an approximation of this station to represent plume materials at 77 seconds after plume release. The filter section collecting PBM was analysed separately to sections of the active sampler collecting GEM. The sampler was analysed to have collected 9.5 ng g^{-1} GEM while the filter from this sample contained PBM below the detection limit of the analytical method (0.1 ng g^{-1}). Therefore, PBM at this site is < 1% of THg.

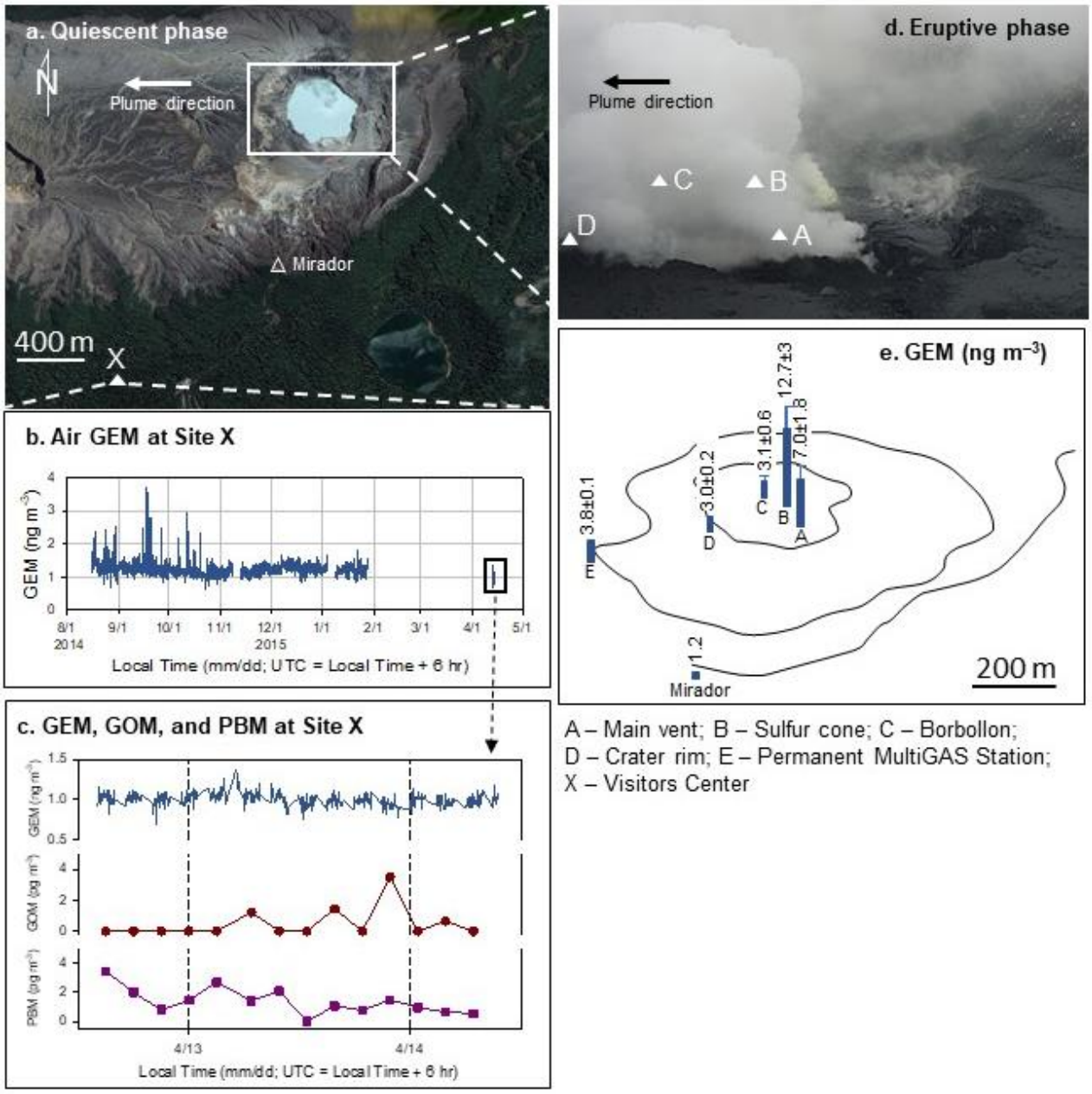

Figure 3.3: Poás Volcano during the quiescent (a) and active (d) phases. Panels b) shows the duration which GEM was collected at site X and concentrations during the sampling period during the quiescent phase in 2014-2015. Panel c) shows the concentrations of gaseous elemental mercury (GEM), gaseous oxidized mercury (GOM) and particulate-bound mercury (PBM) measured at the Visitors Centre (Station X) during the timeframe identified in panel (b). Panel (e) shows the GEM concentration in atmospheric samples at each site within Poás during the active phase of 2017.

Table 3.3: Volcanic GEM concentrations for passive and active samplers between each sampling site (ND indicates no data).

Sampling site (Letter on figure 3.3)	Method	Range of sampling duration	Mean GEM (ng m^{-3}) (range, SD, n)	SO_2* (ng m^{-3})	GEM/SO_2	ΦHg (kg a^{-1})
Main Vent (A)	Active	2 – 3 h	7.8 (16.8 – 2.0; 7.9; 3)			
	Active (for Hg/SO_2)	3.3 h	4.49 (n=1)	3.2×10^7	1.4×10^{-7}	99
	Passive	7 d	6.4 (5.2 – 8.0; 1.4; 4)			
Sulphur Cone (B)	Active	40 min	24.2 (1)	ND	ND	ND
	Passive	7 d	9.8 (8.5 – 12.9; 2.1; 4)			
Borbollón (C)	Active	ND	ND	ND	ND	ND
	Passive	7 – 9 d	3.4 (2.1 – 4.9; 1.3; 4)			
Crater Rim (D)	Active	2 – 3 h	3.1 (1.9 – 3.9; 0.9; 3)	ND	ND	ND
	Active (long duration)	33 h	3.1 (1)			
	Passive	7 – 17 d	2.8 (2.1 – 3.1; 0.4; 7)			
Permanent MultiGAS (E)	Active	ND	ND	ND	ND	ND
	Passive	11 d	3.8 (3.7 – 3.9; 0.1; 2)			
Interoperative Center (X)	Active (at mirador)	3 h	1.2 (1)	ND	ND	ND
	Passive	24 d	1.2 (1.2 – 1.2; 0.04; 3)			

* Estimated from total sulphide analysis.

3.3 Mercury fluxes from Poás

Assuming a fixed ratio of Hg/SO_2 can be used to estimate volcanic Hg emissions as commonly done in the literature (Pyle and Mather, 2003; Nriagu and Becker., 2003) (the validity of this approach is discussed in Chapter 4), an estimate can be made on the Hg flux during the active phase of Poás. An atmospheric concentration of 4.7×10^7 ng m^{-3} SO_4^{2-} was determined from a bubbler sample at the main vent (Table 3.3). Simultaneous monitoring from a permanent MultiGAS station during the initial portions of the active phase of Poás measured a H_2S/SO_2 molar ratio of < 0.01 (de Moor et al., 2017) suggesting that H_2S was negligible compared with SO_2. Therefore, SO_2 concentration can be calculated as 3.2×10^7 ng m^{-3}. The corresponding atmospheric Hg sample simultaneously taken during this period was 4.49 ng m^{-3} (sample CR1-A-2; Appendix 2). The corresponding Hg/SO_2 mass ratio measured from the main vent may then be calculated as 1.4×10^{-7}. Total SO_2 emissions from Poás during the active phase measured by a

drone-mounted DOAS were ~1944 t day^{-1} (de Moor et al., 2017). Extrapolating from the provided daily sulphur flux and calculated Hg/SO_2 mass ratio yields a total Hg flux for Poás volcano during the sampled active phase of 272 g day^{-1}, or 99 kg a^{-1}.

3.3 References

De Moor, J.M., Aiuppa, A., Avard, G., Diaz, J.A., Corrales, E., Rudiger, J., D'Arcy, F., Fischer, T.P., Stix, J., and Alan, A. (2017): A Sulfur Trigger for the 2017 Phreatomagmatic Eruption of Poas Volcano, Costa Rica? Insights from MultiGAS and Drone-based Gas Monitoring; American Geophysical Union. Fall Meeting 2017, abstract #V23F-04

Nriagu, J.O. and Becker, C. (2003): Volcanic Emissions of Mercury to the Atmosphere: Global and Regional Inventories; Science of The Total Environment. Volume 304, pages 3-12.

Pyle, D.M. and Mather, T.A. (2003): The importance of volcanic emissions for the global atmospheric mercury cycle; Atmospheric Environment. Volume 37, pages 5115-5124.

Chapter 4: Discussion

4.1 Comparison of Hg in water and ash from Poás and Turrialba volcanoes

Mercury concentrations in the water of the Poás crater lake (1.2 – 7.6 ng L^{-1}) suggest that even during the quiescent periods of this volcano, Hg is not present in the volcanic gases at high concentrations. This concentration range is one order of magnitude lower than that measured at Turrialba (72.5 ng L^{-1}). The only literature value on Hg in volcanic lakes is the Ruapehu crater lake where the Hg concentration was reported to be 430 ng L^{-1} (Deely and Sheppard, 1998) (Table 4.1), which is one or two orders of magnitude higher than that measured at Turrialba and Poás, respectively. During a field school in August 2018 which was unrelated to this work, I collected a water sample at a hydrothermal field adjacent to Mutnovesky volcano, Russia, and the Hg concentration was 68.6 ng L^{-1} (n=1), similar to that of Turrialba but ~10 times that of Poás. Overall, aqueous Hg concentrations at Poás are typical of a North American freshwater system, and concentrations at Turrialba are within the range of contaminated environments from mining (Scudder et al. 2009).

Corresponding to observations in water concentrations, Hg concentrations in ash are an order of magnitude lower at 200 m away from the plume of the main vent at Poás than at a comparable location for Turrialba (Table 4.1). Samples from Poás comprised of only volcanic ash were within the range of comparable volcanic ash samples directly from the main vent (Coufalík et al., 2018), and over 200% higher further downplume (Figure 3.1). Ash collected from Turrialba at 200 m is over 26 times higher than other collected ash samples. Both ash samples from Poás and Turrialba are also elevated (165% at 0 m from the main vent; 459% at 200 m; 628% at 400 m) when compared with the average Hg concentration in the continental crust (2.9 ng g^{-1}; Canil et al., 2015); however, it is important to note that Hg is not homogenously distributed in the crust and is known to be higher in lithologies containing high proportions of clay minerals and organic matter

(Wedepohl, 1995). Ash from Poás is lower in Hg than typical clay mineral-rich rocks, and ash from Turrialba falls within typical values (110 – 200 ng g^{-1}; Srivastava, 1979). Hg in sulphur from the borbollón 165.6 ng g^{-1} and cinder cone 14.6 ng g^{-1} of Poás during the active phase is near the lower margins of what has been documented in other deposits of elemental volcanic sulphur (11 – 9300 ng g^{-1}; Srivastava, R.K., 1979). This is likely because Hg acts as a moderately volatile element which tends to be fully degassed from magmas as GEM and is oxidized and sorbed onto the surface of the particles.

Table 4.1: Hg concentrations in the volcanic environment of Poás and Turrialba, and comparison with literature values for other volcanic sources.

Hg in Component	Poás	Turrialba	Other Sources
Water (ng L^{-1})	7.6; 1.2	72.5	68.6 (Mutnovesky) 430 (Ruapehu)*
Ash (ng g^{-1})	13.3	160.0	0.3 – 6.0 (Volcanic Ash)**
Atmospheric (ng m^{-3})	7.0 ± 1.8	115† 81 (76 – 85) †	6 (Poas)† 99 – 125 (Etna)† 4 (Gorely)† 8 – 40 (Mutnovsky)† 8 (Aso Crater Lake)† 119 (Aso)† 5 (Rincon de la Vieja)† 140 – 530 (Las Pilas)† 145-1329 (Las Hornillas)† 28 – 325 (Miyakejima)†† 27 – 55 (Asama)†† 122 – 611 (Nyiragongo)†† 19 – 142 (Yasur)†† 29 – 167 (Ambrym)†† 18 (La Soufriere Hill)†† 101.7 – 225.0 (Masaya)†††

*Deely and Sheppard (1998); ** Coufalík et al., (2018); †Bagnato et al., (2014); ††Bagnato et al., (2011); †††Witt et al. (2008)

Higher concentrations of Hg in collected sulphur at the borbollón of Poás signify that at this location, Hg may not be emitted as a gas and is instead retained in solution. This is likely due to the chalcophile affinity of Hg (Canil et al., 2015). Concentrations of Hg in ash are anomalously

higher surrounding this feature than at the main vent and are most likely due to the expulsion of material in the surrounding area. Only the immediate area is suspected to contain ejecta from this feature. Observations made during field work did not show any interaction between the degassing of the borbollón and the plume from the main vent. Furthermore, the air above the borbollón contains the lowest measured concentrations of GEM at the crater of Poás, suggesting that Hg is retained in the material instead of being pyrolyzed into the atmosphere. While these observations may hold for the borbollón, it is difficult to make comparisons between others features present on the crater floor or to relate Hg emissions between all features present at the crater of Poás. The spatial concentration and distribution of Hg has been documented to be extremely heterogenous in volcanic environments (Lescinsky et al., 1987; Bagnato et al., 2014).

4.2 Passive samplers for Hg measurements in volcanic gases

The deployment of passive samplers in this study represents the first attempt to use iodated active carbon samplers or sulphated passive carbon samplers in a volcanic environment and the first comparative study of passive and active samplers at volcanoes. Previous work (Bagnato et al., 2014, 2018; Aiuppa et al., 2007; Witt et al., 2008) has concentrated on active samplers or in a few cases real-time measurements. While such monitoring techniques provide high temporal resolution data to study the dynamics of volcanic emissions, they require either external power that may not be available or batteries that may not be reliable or long-lasting. They also require researchers to spend sufficiently long time (at least several hours) in a hazardous environment (Bagnato et al., 2014; Aiuppa et al., 2007). Passive samplers that do not require power or maintenance may be a viable alternative and allow for a better global knowledge of individual volcanoes.

The passive devices used in this study are inexpensive, lightweight, and easily deployed with little training required in Hg sampling (McLagan et al., 2015). As shown in Chapter 3, passive

and active samplers deployed side by side in Poás yielded air Hg concentration data that were statistically indistinguishable. While it is understood that a direct comparison between the two techniques is hindered by the different sampling durations involved, these results suggest that passive sampling is a promising technique for measuring volcanic Hg emissions when compared with active sampling, as has been observed under more typical urban and rural conditions (McLagan et al. 2018). To have more confidence in the passive sampler, a larger sample size of comparisons is needed, especially of active samplers collecting over the same long duration as the passive samplers or with the aid of a real-time monitoring instrument. It is our recommendation that validation of the efficacy of passive sampling in this context be conducted in the field at an easily accessible site close to, and downplume of a degassing feature. Masaya volcano has been the site of other major gas studies (Martin et al., 2012, 2010; Witt et al., 2008) and is easily accessible (Global Volcanism Program, 2017) presenting a good site for additional validation. Upon further proof, we believe that there is a possibility of including these devices to collect at permanent gas monitoring stations of volcanoes which do not yet have an established Hg/SO_2 ratio. This would allow for a larger sample size then currently exists (Bagnato et al., 2014) when inferring global volcanic Hg trends.

4.3 Atmospheric concentrations and mercury flux from Poás over phases of activity

An important knowledge gap regarding volcanic Hg emissions comes from a lack of measurements during active phases in volcanic eruptions. The assumption that plumes of explosive degassing have a larger Hg/SO_2 ratio compared to plumes of passive degassing is based on the limited measurements of Varekamp and Buseck (1986), and further extrapolated from ice or snow layers such as in Zdanowicz et al. (2015). A recent study suggested that high Hg layers in ice cores which have been previously correlated to explosive volcanic events may be misattributed because of core chronology problems (Chellman et al., 2017). The larger Hg/SO_2 ratio attributed to erupting

volcanoes remains a substantial factor in determining the magnitude of annual volcanic Hg emissions within commonly cited estimations (Nriagu and Becker, 2003; Pyle and Mather, 2003). The total volcanic Hg flux derived from this assumption often eclipses the total value attributed to passive degassing despite no direct measurements having been reported during an active phase of volcanism (Pyle and Mather, 2003; Bagnato et al., 2014).

The measured Hg flux from Poás is 97.4 kg a^{-1} greater over the active phase than that calculated by Bagnato et al. (2014) (Table 4.2). Between active and passive phases, the Hg/SO_2 ratio measured directly from the main vent increased (passive phase: 3.7×10^{-8} in Bagnato et al., 2014; active phase: 1.4×10^{-7} in this work). Such an observation agrees with the concept that the Hg/SO_2 ratio will increase during volcanic eruptions (Pyle and Mather, 2003; Nriagu and Becker, 2003). Even though the Hg/SO_2 ratio increased at Poás during active degassing, it is still two orders of magnitude lower than the range given in Pyle and Mather (2003) of 10^{-5} to 2×10^{-4} for eruptive volcanoes, and an order of magnitude lower than the range given for passively degassing volcanoes of 10^{-6} – 10^{-4}, signifying that Poás is a low Hg emitting volcano over both stages of activity compared with other volcanoes.

This study presents the first series of measurements to be carried out during two phases of volcanic activity directly from the main plume and suggests that Hg and SO_2 may not share the same geological sources or emission processes. If Hg and SO_2 do act independently, then the assumption that there will be a higher Hg/SO_2 ratio during eruptive phases may not be valid across all volcanic eruptions. The measurements presented in this work suggest, at least, that the presumption of an order of magnitude higher Hg/SO_2 ratio for active degassing does hold true for Poás. Further validation is needed for other volcanoes to investigate whether this tentative conclusion holds true for other volcanoes. Adopting a more conservative measure of volcanic Hg

flux using the same Hg/SO_2 ratio over all stages of volcanic activity may be most prudent until more volcanoes have been examined over different stages of activity. Using the same Hg/SO_2 ratio over multiple phases of volcanic activity would result in a global Hg flux from active volcanic sources being an order of magnitude lower than the value reported by Pyle and Mather (2003), and a significant reduction in active sources in global flux calculations by Nriagu and Becker (2003). Global flux estimations from passive degassing in Bagnato et al. (2014) and Nriagu and Becker (2003) would remain unchanged. Of additional note is the finding that the CO_2 flux during this period did not increase by the same magnitude as SO_2 (see Table 4.2; a 15-fold increase in SO_2 and a 4-fold increase in CO_2) which suggest that CO_2 may be more strongly correlated to Hg emissions and a better tracer gas for future estimations. A stronger correlation has also been measured in comparative Hg vs. SO_2 and Hg vs. CO_2 measurements at Volcano, Italy, which show a stronger correlation to CO_2 ($r^2 = 0.80$ for CO_2 and 0.66 for SO_2; Aiuppa et al., 2007).

Table 4.2: Hg and major gas fluxes over different phases of volcanic activity.

Year Measured	Poás Hg concentration ($ng\ m^{-3}$)	Poás Hg/SO_2 ratio (wt.)	Hg flux ($kg\ a^{-1}$)	SO_2 flux ($t\ d^{-1}$)**	CO_2 flux ($t\ d^{-1}$)**
2013	6.0 ± 1.2*	3.7×10^{-8}*	1.6*	130	49
2015 (this study)	1.2	ND	ND	40	54
2017 (this study)	7.0 ± 1.8	1.4×10^{-7}	99	1944	204

*Bagnato et al., 2014; **provided by De Moor, J.M. (unpublished data)

4.4 An eruption frequency-based model

We now turn to the critical question of why Poás emits such a low amount of Hg when compared with Turrialba and other volcanoes, and especially why GEM concentrations from an active plume were not substantially elevated when compared with the background. Trace elements in the volcanic emissions may originate directly from magma, from pyrolyzation or erosion of crustal materials that the high-temperature magma comes in contact with as it ascends, or from

leaching of surface rocks by condensed acid liquids produced from the mixing of magmatic gases with meteoric water. Hg may also be removed by precipitation as magma or fluids cool down and via scrubbing by acidic crater lakes (Symonds and Reed, 2001; Symonds et al., 1992). Although the abundance of Hg in the mantle remains poorly studied (Canil et al., 2015), the mantle is expected to be strongly depleted in Hg when compared with the crust, as Hg in the high-temperature mantle would be virtually exclusively present as the gaseous Hg^0 which is lost over geological time. This suggestion is supported by a recent estimate of an average Hg concentration of 0.4 – 0.6 ng g^{-1} in the primitive upper mantle (Canil et al., 2015), which is two orders of magnitude lower than the estimated average Hg concentration in the crust (40 ng g^{-1} (Wedepohl, 1995); 2.9 ng g^{-1} (Canil et al., 2015)). As the hot magma ascends, Hg present in crustal materials (primarily Hg^{2+}) would be readily pyrolyzed to Hg^0 and mixed into the gas emissions. This is especially important as much higher concentrations of total Hg, often > 500 ng g^{-1}, are found in certain rock layers in the upper crust, such as coal, shale, and other sediments rich in organic carbon or clay minerals (Bragg et al., 1998; Cameron and Jonasson, 1972). Large amounts of Hg deposited in concentrated areas, either as cinnabar or associated minerals, are also geospatially related to volcanic processes (Rytuba, 2003). Therefore, the in-plume concentration of volcanic Hg is likely controlled by the amount of crustal Hg that is assimilated by the rising magma.

While both volcanoes investigated in this study were in active stages of degassing, different eruptive dynamics are represented at each location. Poás is one of the most active volcanoes in the world and is typified by frequent, smaller phreatic eruptions (hundreds per year (de Moor et al., 2016a)) while Turrialba exhibits less frequent, larger eruptions with longer repose time between eruptions (> 100 years (de Moor et al., 2016b; Reagan et al., 2006)). As such, Poás represents a high-frequency eruption setting where the Hg-containing crustal rocks that the plume interacts

with have been in prolonged contact with high-temperature magma and fluids during many previous eruptions. In contrast, Turrialba represents a moderate-frequency eruption environment in which the rocks surrounding the plume have not been as exposed to high-temperatures. By this process, volcanoes with a high frequency of eruptive events will have prolonged periods of interaction with Hg-rich units, and over time, will deplete Hg in these units and no longer produce an Hg-rich plume (Figure 4.1). Volcanoes with a low frequency of eruptive events will have limited periods of interaction with Hg-rich units and may retain the ability to produce an Hg-rich plume during eruptive phases. Poás has a low N_2/He ratio and negative $\delta^{15}N$ consistent with a mantle-sourced magma while Turrialba indicates a small portion of the magma is derived from melting of subducted ocean sediments (Fischer et al., 2002). Similarly, $\delta^{13}C$ values from a global compilation of volcanoes (Mason et al., 2017) show values for Poás magma that indicate no crustal contamination during ascent, and slight contamination for Turrialba.

Higher Hg concentrations at Poás in both ash and atmospheric samples collected from the sulfur cone compared to the main vent are a possible indicator of this model's validity. Changes in the thermal gradient during an eruptive phase of Poás of 1988-1989 (Oppenheimer and Stevenson, 1989) removed the overlying lake and exposed pools of liquid sulphur at the crater floor. This phenomenon occurs as the result of a new eruptive phase, changing the thermal gradient to remobilize native sulphur precipitated within lake sediments. At the end of the eruptive phase, thermal gradients in lake sediments would have then declined to previous levels. Clay-sized material analysed within this study is determined to have settled to the lake floor from periods of low agitation. Absorption/adsorption of Hg onto these suspended clay particles has led to higher Hg concentrations than surrounding material (see Figure 3.1). Hg deposited in lake sediments in new layers would then be pyrolyzed and transported under the same mechanisms as the pools of

native sulphur. Thus, newer units interacting with fluids are enriching the fumaroles, while the main vent which has not experienced significant Hg deposition between eruptive phases remains depleted in Hg. This eruptive frequency hypothesis would also suggest that past extrapolations of volcanic Hg emissions drawn analysis from fumaroles (Bagnato et al., 2014; Ferrara et al., 2000; Pyle and Mather, 2003) may not be representative of the bulk volcanic emissions from the main vent.

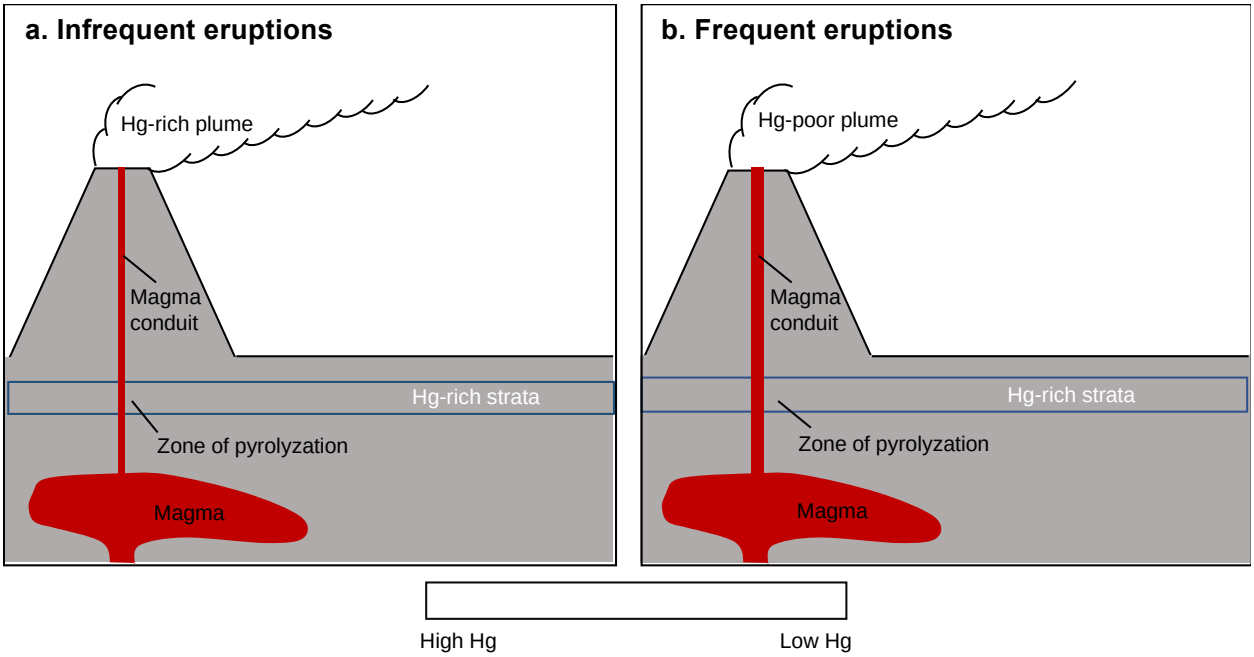

Figure 4.1: Conceptual endmembers of a low and high plume-Hg volcanic system. High plume-Hg volcanic systems (left) are less active and experience infrequent eruptions. Less interaction with magma and fluids creates a narrow zone of existing Hg pyrolyzation within Hg-enriched strata (blue). Fresh magmatic/fluid interaction has great potential to incorporate Hg resulting in a Hg-rich plume. Low plume-Hg volcanic systems (right) are more active and experience frequent eruptions. Extensive interaction with magma and fluids creates a wide zone of existing Hg pyrolyzation within Hg-enriched strata (blue). Fresh magmatic/fluid interaction has limited ability to incorporate Hg further resulting in a Hg-poor plume.

4.5 Global mercury emissions inferred from eruptive frequency

To test the validity and applicability of this model, we analyzed available literature of volcanic eruptions (Global Volcanism Program, 2013) with published Hg/SO_2 measurements and database of recorded eruptive events, then plotted Hg/SO_2 against the eruption frequency over the past 200 years. 200 years was chosen as an arbitrary benchmark for this comparison due to data availability. The use of SO_2 as a tracer gas to test the validity of this model and to extrapolate towards a global volcanic Hg emission is necessary due to limited information about other major gases (e.g., CO_2). Even though CO_2 has been demonstrated as more strongly correlated to Hg (Aiuppa et al., 2007) there are fewer Hg/CO_2 data available than for Hg/SO_2 (Bagnato et al., 2013, 2018). SO_2 emissions from volcanic sources are monitored using satellite measurements (Carn et al., 2017; Andres and Kasgnoc, 1998) whereas volcanic CO_2 emissions are either extrapolated from gas fluxes which may be measured from a satellite (SO_2 most commonly but CO and H_2S may be detected (Martinez-Alonso et al., 2012; Clarise et al., 2011)) or analysed *in situ* (Bagnato et al., 2018). As such, the CO_2 fluxes are often not measured from eruptive events (Global Volcanism Program, 2013), which limits the power of a model constructed from Hg/CO_2 ratios.

A few additional caveats must be highlighted to emphasise the limitations of this model:

i. Not all smaller eruptive events are necessarily recorded for all volcanoes. For example, the database used in this study reports 51 eruptions for Poás (Global Volcanism Program, 2013) yet hundreds of individual phreatic to phreatomagmatic eruptions have occurred since the initiation of the present phase of activity in 2006 (de Moor et al., 2016a), leading to some underestimation of eruptive frequency.

ii. Due to the limited number of volcanoes for which Hg/SO_2 ratios have been measured, there is a small sample size considering the total number of volcanoes which exist.

iii. The Hg/SO_2 ratios were measured by various methods (Bagnato et al., 2014; Ferrara et al., 2000; Kyle et al., 1990; Varekamp and Buseck, 1986) of sample collection and analysis. Most Hg data represent discrete sample collection followed by analysis *ex situ*, whereas a few were made by *in situ* in real-time using a portable Hg analyzer (Aiuppa et al., 2007; Bagnato et al., 2014). Most of the SO_2 data were measured by real-time using a portable MultiGAS analyzer. Note also that some of the measurements were of GEM, whereas others were of TGM which may include other gaseous Hg species. Here we combine them as Hg because in volcanic emissions GEM is the dominant form (Bagnato et al., 2014).

iv. Some of the Hg/SO_2 ratios were measured in volcanic plumes (Bagnato et al., 2011; Bagnato et al., 2014; Mather et al., 2012; Wardell et al., 2008; Witt et al., 2008), and others in fumarolic condensates (Bagnato et al., 2014; Ferrara et al., 2000; Varekamp and Buseck, 1986). These two types of measurements may not provide consistent Hg compositions for the same volcanic system, as both Hg and SO_2 may undergo different chemical processing in fumarolic emissions than in high-temperature plume emissions directly from magma (Aiuppa et al., 2007; Symonds et al., 1992).

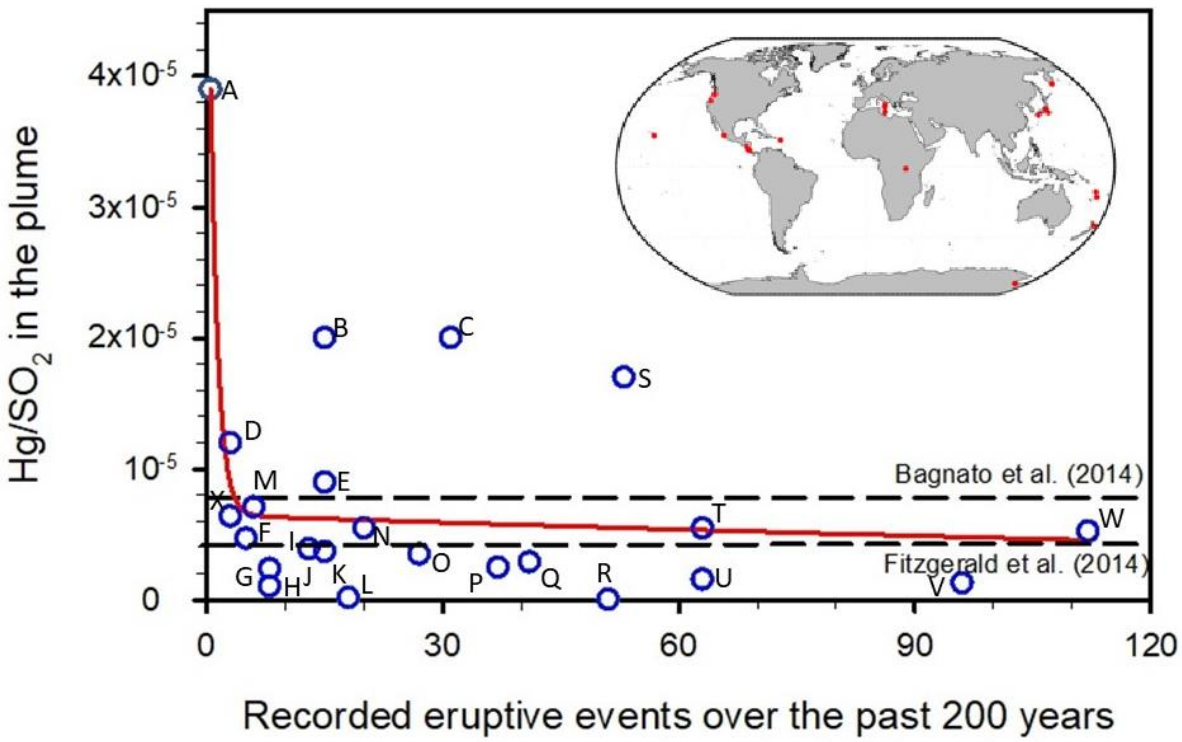

Figure 4.2: Relationship between the Hg/SO_2 ratio in volcanic plume and the eruptive frequency for 24 volcanoes which data is available. The red line represents an exponential decay relationship. A-Mt. Shasta; B-Erebus; C-Masaya; D-La Soufriere Hill; E-Miyakejima; F-Mt. Hood; G-Stromboli; H-Vulcano (B); I-Vulcano (A); J-Turrialba; K-Gorely; L-Mutnovsky; M-St. Helens; N-Nyiragongo; O-Rincon de la Vieja; P-Colima; Q-White Island; R-Poas; S-Yasur; T-Asama; U-Kilauea; V-Aso; W-Etna; X-Ambrym. The inset map shows the locations of the volcanoes. The detailed data and data source can be found in Appendix 2.

With the above caveats, the resulting plot of the Hg/SO_2 ratio against eruption frequency from available data shows a general decrease in the Hg/SO_2 ratio with increasing eruption frequency (Figure 4.2). The overall trend is strongly biased by one single data point (A, Mt. Shasta), which is the least eruptive volcano with the highest Hg/SO_2 ratio. Statistically this point would have been shown as an outlier; however, we could not rule out this data point as it agrees very well with what predicted from the new conceptual model (Figure 4.1). Including this data point in the curve fitting, the following relationship can be obtained:

$$\frac{[Hg]}{[SO_2]} = \left(5.45\times10^{-5}\, e^{-1.0\times f}\right) + \left(6.51\times10^{-6} e^{-3.1\times10^{-3}\times f}\right) \quad (r^2 = 0.59;\ n = 24) \quad (1)$$

where f is the number of eruptions over the past 200 years. For an inactive volcano, the first eruption will readily mobilize a large amount of Hg, resulting in a very high Hg/SO_2 ratio within the plume. As the eruption frequency increases, our hypothesis states that there would be significantly less Hg available for mobilization, and the Hg/SO_2 ratio would decrease on a more gradual scale. This two-phase decreasing trend of Hg/SO_2 with increasing eruption frequency is consistent with our model (Figure 4.1) and best described by equation (1). As the Hg emissions from volcanoes are tentatively dependent on eruption frequency, the current practice of using a single, average Hg/SO_2 ratio to estimate global volcanic Hg fluxes may be inappropriate. For instance, the average Hg/SO_2 ratio of 7.8×10^{-6} (Bagnato et al., 2014) is only valid for volcanoes that erupt once or twice over the past 200 years, and thus overestimate Hg emissions from the vast number of volcanic sources (Figure 4.2)

Again, it should be noted that equation (1) is heavily weighted by one data point (A in Figure 4.2), and would strongly benefit from more measurements from sources with few eruptions over 200 years. Anomalously high or low measurements which also exist include points B, S, C, and R (see Figure 4.2). Potential processes to explain these outliers are leaching of surface rocks by condensed acid liquids, and differential scrubbing of Hg and SO_2 by acidic crater lake waters to form $HgCl_2$ and H_2SO_4 (Symonds et al., 1993; Symonds and Reed, 2001). Outlying points may also be explained as measurements taken at a distance away from the source of the volcano (Witt et al., 2008). Extrapolating an Hg/SO_2 ratio from a sufficiently far site would include measurements of background atmospheric Hg incorporated into the plume, while SO_2 is only diluted with distance, resulting in an overestimated Hg/SO_2 ratio. The process of atmospheric dilution is demonstrated by atmospheric GEM measurements from Poás in this study, where the concentration of Hg is of the same order of magnitude at ~200 m and ~400 m (Figure 3.3) while

the concentration of SO_2 decreases by over an order of magnitude at the same stations (de Moor, pers. comm.). An Hg/SO_2 ratio measured at the furthest point along the transect would be higher than an Hg/SO_2 ratio measured at the intermediate point of the transect simply due to a lower concentration of SO_2 (see Figure 3.3).

Should equation (1) stand, it is possible to calculate a new global flux based on compiled emission data from a decade of volcanic eruptions (Global Volcanism Program, 2013; Appendix 3). The new flux assumes that the Hg/SO_2 ratio of a volcano will plot on the curve (Equation 1) based on the number of eruptive events recorded in the Global Volcanism Program (2013) database over 200 years and that the Hg/SO_2 ratio of an eruptive event will not differ between passive and active degassing. By these assumptions, we find that the lower threshold for the total annual volcanic Hg flux from eruptive activity over the 10-year period of 2006 – 2015 to be 30 ± 39 t a^{-1} (Appendix 3). This value is ~50% of the global volcanic Hg emission from passive degassing estimated by Bagnato et al. (2014), and only ~5% of the global volcanic Hg emission from active eruptions estimated by Pyle and Mather (2003). Therefore, should our conceptual model hold true, the annual Hg emissions from global volcanic activities would be much less than we previously thought. It is thus important that further studies be carried out, especially at volcanoes that are less frequently erupting, to validate the model and to improve the estimate on global volcanic Hg emissions.

4.6 References

Aiuppa, A., Bagnato, E., Witt, M.L.I., Mather, T.A., Parello, F., Pyle, D.M., and Martin, R.S. (2007): Real-time simultaneous detection of volcanic Hg and SO_2 at La Fossa Crater, Volcano (Aeolian Islands, Sicily); Geophysical Research Letters. L21307, doi:10.1029/2007GL030762.

Andres, R.J. and Kasgnoc, A.D. (1998): A time-averaged inventory of subaerial volcanic sulfur emissions; Journal of Geophysical Resresearch-Atmosphere. Volume 103, pages 25251–25261.

Bagnato, E., Aiuppa, A., Parello, F., Allard, P., Shinohara, H., Liuzzo, M., and Guidice, G. (2011): New clues on the contribution of Earth's volcanism to the global mercury cycle; Bulletin of Volcanology. Volume 73, pages 497–510.

Bagnato, E., Tamburello, G., Aiuppa, A., Sprovieri, M., Vougioukalakis, G.E., and Parks, M. (2013): Mercury emissions from soils and fumaroles of Nea Kameni volcanic center, Santorini, Greece; Geochemical Journal. Volume 47, pages 437-450.

Bagnato, E., Tamburello, G., Avard, G., Martínez-Cruz, M., Enrico, M., Fu, X., Sprovieri, M., and Sonke, J.E. (2014): Mercury fluxes from volcanic and geothermal sources: an update; In: The Role of Volatiles in the Genesis, Evolution and Eruption of Arc Magmas. Zellmer, G.F., Edmonds, M., and Straub, S.M., editors; Special Publications, 410. Geological Society, London. 24 pages, doi: 10.1144/SP410.2.

Bagnato, E., Viverios, F., Pacheco, J.E., D'Agostino, F., Silva, C., and Zanon, V. (2018): Hg and CO_2 emissions from soil diffuse degassing and fumaroles at Furnas Volcano (Sao Miguel Island, Azores): Gas flux and thermal energy output; Journal of Geochemical Exploration. Volume 190, pages 39-57.

Bragg, L.J., Oman, J.K., Tewalt, S.J., Oman, C.L., Rega, N.H., Washington, P.M., and Finkelman, R.B., 1998, The U.S.Geological Survey Coal Quality (COALQUAL) Database -- Version 2.0: U.S. Geological Survey Open-File Report 97-134.

Cameron, E.M. and Jonasson, I.R. (1972): Mercury in Precambrian Shales of Canadain Shield. Geochimica et Cosmochimica Acta; Volume 36, pages 985–1005.

Canil, D., Crockford, P.W., Rossin, R., and Telmer, K. (2015) Mercury in some arc crustal rocks and mantle peridotites and relevance to the moderately volatile element budget of the Earth; Chemical Geology. Volume 396, pages 134-142.

Carn, S. A., Fioletov, V. F., McLinden, C. A., Li, C., and Krotkov, A. (2017): A decade of global volcanic SO2 emissions measured from space; Scientific Reports. Volume 7, doi: 10.1038/srep44095.

Chellman, N., McConnell, J.R., Arienzo, M., Pederson, G.T., Aarons, S.M., and Csank, A. (2017): Reassessment of the Upper Fremont Glacier Ice-Core Chronologies by Synchronizing of Ice-Core-Water Isotopes to a Nearby Tree-Ring Chronology; Environmental Science and Technology. Volume 51, pages 4230-4238.

Clarise, L., Coheur, P.F., Chefdeville, S., Lacour, J.L., Hurtmans, D., and Clerbaux, C. (2011): Infrared satellite observations of hydrogen sulfide in the volcanic plume of the August 2008 Kasatochi eruption; Geophysical Research Lettters. Volume 38, doi:10.1029/2011GL047402.

Coufalik, P., Krimicek, L., Zyerina, O., Meszarosova, N., Hladil, J., and Komarek. J. (2018): Model of Mercury Flux Associated with Volcanic Activity; Bulletin of Environmental Contamination and Toxicology; Volume 101, pages 549-553.

de Moor, J.M., Aiuppa, A., Pacheco, J., Avard, G., Kern, C., Liuzzo, M., Martínez, M., Giudice, G., and Fischer, T.P. (2016a): Short-period volcanic gas precursors to phreatic eruptions: insights from Poás Volcano, Costa Rica; Earth and Planetary Science Letters; Volume 442, pages 218-227.

de Moor, J.M., Aiuppa., A., Avard, G., Wehrmann, H., Dunbar, N., Muller, C., Tamburello, G., Giudice, G., Moretti, R., Conde, V., and Galle, B. (2016b): Turmoil at Turrialba Volcano (Costa Rica): Degassing and eruptive processes inferred from high-frequency gas monitoring; Journal of Geophysical Research Solid Earth. Volume 121, pages 5761-5775.

Deely, J.M. and Sheppard, D.S. (1996): Whangaehu River, New Zealand: geochemistry of a river discharging from an active crater lake; Applied Geochemistry. Volume 11, pages 447-460.

Ferrara, R., Mazzolai, B., Lanzillotta, E., Nocaro, E., and Pirrone, N. (2000): Volcanoes as emission sources of atmospheric mercury in the Mediterranian basin; The Science of the Total Environment. Volume 259, pages 115-121.

Fischer, T. P., Hilton, D. R., Zimmer, M. M., Shaw, A. M., Sharp, Z. D., and Walker, J. A. (2002): Subduction and recycling of nitrogen along the central American margin, *Science*. Volume 297, pages 1154-1157.

Global Volcanism Program (2013): Volcanoes of The World, v.4.7.0. Venzke, E (ed.); Smithsonian Institute; Downloaded 13 May, 2018. <http://dx.doi.org/10.5479/si.GVP.VOTW4-2013>

Global Volcanism Program (2017): Report on Masaya (Nicaragua), Smithsonian Institution; Venzke, E. (ed.); Bulletin of the Global Volcanism Network. Volume 42, number 9. <https://volcano.si.edu/showreport.cfm?doi=10.5479/si.GVP.BGVN201709-344100>

Kyle, P.R., Meeker, M., and Finnegan, D. (1990): Emission rates of sulfur dioxide, trace gases and metals from Mount Erebus, Antarctica; Geophysical Research Letters. Volume 17, pages 2125-2128.

Lescinsky, D.T., Connor, C., and Stoiber, R.E. (1987): Soil Mercury Study of Thermal Areas, Rincón de la Vieja Volcano, Costa Rica; Geothermics. Volume 16, pages 159-168.

McLagan, D.S., Mitchell, C.P.J., Huang, H., Lei, Y.D., Cole, A.S., Steffan, A., Hung, H., and Wania, F. (2015): A high-Precision Passive Air Sampler for Gaseous Mercury; Environmental Science and Technology Letters. Volume 3, pages 24-29.

McLagan, D.S., C.P.J. Mitchell, A. Steffen, H. Hung, C. Shin, G.W. Stupple, M.L. Olson, W.T. Luke, P. Kelley, D. Howard, G.C. Edwards, P.F. Nelson, H. Xiao, G.-R. Sheu, A. Dreyer, H. Huang, B. Abdul Hussain, Y.D. Lei, I. Tavchunsky, F. Wania. (2018): Global evaluation and calibration of a passive air sampler for gaseous mercury; Atmospheric Chemistry and Physics. Volume 18, pages 5905-5919.

Martin, R.S., Sawyer, G.M., Spampinato, L., Salerno, G.G., Ramirez, C., Ilyinskaya, E., Witt, M.L.I., Mather, T.A., Watson, I.M., Phillips, J.C., and Oppenheimer, C. (2010): A total volatile Inventory for Masaya Volcano, Nicaragua; Journal of Geophysical Research: Solid Earth. Volume 115, Issue B9, doi:10.1029/2010JB007480

Martin, R.S., Sawyer, G.M., Day, J.A., LeBlond, J.S., Ilyinskaya, E., and Oppenheimer, C. (2012): High-resolution size distributions and emission fluxes of trace elements from Masaya volcano, Nicaragua; Journal of Geophysical Research: Solid Earth. Volume 117, pages

Martinez-Alonso, S., Deeter, M.N., Worden, H.M., Clerbaux, C., Mao, D., and Gille, J.C. (2012): First satellite identification of volcanic carbon monoxide; Geophysical Research Letters. Volume 39 doi:10.1029/2012GL053275

Mason, E., Edmonds, M., and Turchyn, A.V. (2017): Remobilization of crustal carbon may dominate volcanic arc emissions; Science. Volume 357, pages 290-294.

Mather, T.A., Witt, M.L.I., Pyle, D.M., Quayle, B.M., Aiuppa, A., Bagnato, E., Martin, R.S., Sims, K.W.W., Edmonds, M., Sutton, A.J., and Ilyinskaya, E. (2012): Halogens and trace metal emissions from the ongoing 2008 summit eruption of Kilauea volcano, Hawaii. Geochimica et Cosmochimica Acta. Volume 83, pages 292–323.

Nriagu, J.O. and Becker, C. (2003): Volcanic Emissions of Mercury to the Atmosphere: Global and Regional Inventories; Science of The Total Environment. Volume 304, pages 3-12.

Oppenheimer, C. O. and Stevenson, D. (1989): Liquid sulphur lakes at Poás volcano; Nature. Volume 372, pages 790-793.

Pyle, D.M. and Mather, T.A. (2003): The importance of volcanic emissions for the global atmospheric mercury cycle; Atmospheric Environment. Volume 37, pages 5115-5124.

Reagan, M., Duarte, E., Soto, G. J., and Fernandez, E. (2006): The eruptive history of Turrialba volcano, Costa Rica, and potential hazards from future eruptions, in *Volcanic hazards in Central America*, edited by W. I. Rose, et al.; Geological Society of America Special Paper. pages. 235–257.

Rytuba, J.J. (2003): Mercury from mineral deposits and potential environmental impact; Environmental Geology. Volume 42, pages 326-338.

Scudder, B.C., Chasar, L.C., Wentz, D.A., Bauch, N.J., Brigham, M.E., Moran, P.W., and Krabbenhoft, D.P. (2009): Mercury in fish, bed sediment, and water from streams across the United States, 1998–2005; U.S. Geological Survey Scientific Investigations Report 2009–5109. 74 pages.

Srivastava, R.K. (1979): The abundance of mercury in rocks, minerals and native sulphur by a microwave-excited argon plasma; Chemical Geology. Volume 27, pages 255-263.

Symonds, R.B., Gerlach, T.M., and Reed, M.H. (2001): Magmatic gas scrubbing: implications for volcano monitoring; Journal of Volcanology and Geothermal Research. Volume 108, pages 303–341.

Symonds, R.B. and Reed, M.H. (2001): Calculation of multicomponent chemical equilibria in gas-solid-liquid systems; calculation methods, thermochemical data, and applications to studies of high-temperature volcanic gases with examples from Mount St. Helens; American Journal of Science. Volume 293, pages 758–864.

Symonds, R.B., Reed, M.H., and Rose, W.I. (1992): Origin, speciation, and fluxes of trace-element gases at Augustine volcano, Alaska: insights into magma degassing and fumarolic processes. Geochimica et Cosmochimica Acta. Volume 56, pages 633–657.

Varekamp, J.C. and Buseck, P.R. (1986): Global Mercury Flux from Volcanic and Geothermal Sources; Applied Geochemistry. Volume 1, pages 65-73.

Wardell, L.J., Kyle, P.R., and Counce, D. (2008): Volcanic emissions of metals and halogens from White Island (New Zealand) and Erebus volcano (Antarctica) determined with chemical traps; Journal of Volcanology and Geothermal Research; Volume 177, pages 734-742.

Wedepohl, K.H. (1995): The composition of the continental crust; Geochimica et Cosmochimica Acta. Volume 59, pages 1217-1232.

Witt, M.L.I., Mather, T.A., Pyle, D.M., Aiuppa, A., Bagnato, E., and Tsanev, V.I. (2008): Mercury and Halogen Emissions from Masaya and Telica Volcanoes, Nicaragua; Journal of Geophysical Research Solid Earth. Volume 113, Issue B6, 15 pages, doi: 10.1029/2007jb005401.

Zdanowicz, C., Kruemmel, E., Lean, D., Poulain, A., Kinnard, C., Yumvihoze, E., Chen, J., Hintelmann, H., (2015): Pre-industrial and recent (1970-2010) atmospheric deposition of sulfate and mercury in snow on southern Baffin Island, Arctic Canada; Science of The Total Environment. Volume 509-510, pages 104-114.

Chapter 5: Conclusions

5.1 Main findings

The main findings from this study are that:

1) Poás is an exceptionally low Hg-emitting volcano, whereas Turrialba represents a moderate Hg-emitting volcano.
2) The Hg/SO_2 ratio from Poás volcano increased during the active phase.
3) Passive samplers of the type used in this study are a promising technique for collecting air samples from volcanic emissions for Hg concentration measurements.
4) A conceptual model is proposed to explain the difference in Hg emissions from Poás and Turrialba. The model postulates that volcanic Hg emissions decrease with increasing eruption frequency.
5) Available literature data in general support the conceptual model, although more studies are needed to measure Hg emissions from volcanoes that are less frequently eruptive.

Based on the model, a new global volcanic Hg emission flux is estimated to be 30 ± 39 t a^{-1} over the 10-year period of 2006 – 2015, which is 50–95% lower than the commonly cited values (Pyle and Mather, 2003; Nriagu and Becker, 2003)

5.2 Future work

A limitation on the model validation presented in this thesis is a lack of data for Hg/SO_2 ratios on the lowest (>5 eruptions over 200 years) and highest (<60 eruptions over 200 years) eruptive frequency end of the curve. Measuring ratios at volcanoes that fall into this range of eruptive frequency would further strengthen the model. If infrequently emitting volcanoes do emit the most Hg, then potential targets for future measurements would include Mt. Fuji and Hakkoda volcanoes in Japan or Katmai volcano in Alaska. Likewise, if the most active volcanoes do not emit large quantities of Hg, a potential target for future measurements would include

Klyuchevskoy volcano, Russia (Global Volcanism Program, 2013). Measurements of both low and high incidences of eruption are important to the model validity. If volcanoes with high eruption frequency are not large emitters, they may form a small fraction of total Hg emissions. If volcanoes with low eruptive frequency are large emitters, they may almost entirely dictate the global volcanic Hg inventory and should be given priority.

Our current understanding of trace metal emissions from volcanoes remains limited, in particular with respect to temporal variations. The implication that volcanic Hg is improperly indexed to SO_2 extends to other trace metals which are present in the plume. This study underscores the need for continued monitoring of at least one volcano for not only major gases, but simultaneous monitoring for a full suite of trace metals to draw larger trends over the course of years. This can be done either through collection of particulate metals on filter paper at a distance from the plume (Martin et al., 2010; 2012), or directly collecting metals in solution (Zelinski et al., 2013).

The implication that Hg seen in the plume is primarily from recycled crustal material requires future work to quantify the exact amount. Poás would provide an excellent ground for isotopic analysis of plume Hg representative of mantle values. A comparison of uncontaminated Poás isotopic ratios to existing samples of volcanic gases (Zambardi et al., 2009) would present an opportunity to further validate the model proposed in this thesis and may present an opportunity to treat Hg as a proxy for magma contamination from the crust in volcanic terrains.

Indications exist from major gas patterns in this study that CO_2 may be a superior normalizing gas for Hg than SO_2. Real time measurements in Aiuppa et al. (2007) show a closer Hg affinity to CO_2 than SO_2 over short-term periods, however this needs to be investigated further to establish long-term patterns related to shifts in volcanic activity. Future research would then

need to examine trends of Hg/SO_2, Hg/CO_2, and SO_2/CO_2 ratios over multiple phases of volcanic activity. The methodology for this would, in effect, be similar to existing research such as de Moor et al. (2016) in extrapolating from major gas trends to forecast shifts of volcanic activity. If the infrastructure and methodology has been developed for long-term major gas investigation, then the only requirement would be to add another device sampling for Hg in the same location. Any such sampler would have to persist in the same environment as existing monitoring stations (usually permanent MultiGAS devices) and most likely operate under low power requirements. As of such, major considerations should be A) Hg sampling method, and B) site selection for monitoring. The Hg sampling method may be either passive samplers used in this study, or long-term Hg monitoring instrumentation (such as a Tekran 2537 unit). Passive samplers require no power source but need days to collect samples, so they do not provide a directly comparable sampling rate to MultiGAS devices which measure at a much higher resolution (minutes). Hg monitoring instruments provide information at a more comparable resolution to MultiGAS analysers but require a power source and the quality of measurements may be easily be degraded by acidic plume gases (Witt et al., 2008). The limitations and strengths of each method should be taken into account before deployment. Any site selected for future work should have existing major gas monitoring infrastructure and be as close to the main vent as possible. As volcanic processes occur over geological time, changes in activity are unpredictable and difficult to detect during the short human timespans during which research is conducted. Because the model presented in this study suggests that very frequently erupting volcanoes will have a low-Hg plume, the major concern with using a frequently erupting volcano as a test site would be the low initial concentrations of Hg in the plume. Balancing the need for a detectable Hg signal well above ambient atmospheric levels and the need for multiple phases of volcanic activity to be measurable,

an intermediately active volcano would be most desirable for future research related to a comparison of Hg/CO_2 and Hg/SO_2 ratios. This research is critical to establish the true flux of Hg during volcanic eruptions, and a larger dataset from these sources would result in more confidence towards the primary global Hg flux.

5.3 References

Aiuppa, A., Bagnato, E., Witt, M.L.I., Mather, T.A., Parello, F., Pyle, D.M., and Martin, R.S. (2007) Real-time simultaneous detection of volcanic Hg and SO_2 at La Fossa Crater, Volcano (Aeolian Islands, Sicily); Geophysical Research Letters. L21307, doi:10.1029/2007GL030762.

Global Volcanism Program (2013): Volcanoes of The World, v.4.7.0. Venzke, E (ed.); Smithsonian Institute; Downloaded 13 May, 2018. <http://dx.doi.org/10.5479/si.GVP.VOTW4-2013>

Martin, R.S., Mather, T.A., Pyle, D.M., Day, J.A., Witt, M.L.I., Hilto, R.G. (2010): Major and trace element distributions around active volcanic vents determined by analysis of grasses: implications for element cycling and bio-monitoring; Bulletin of Volcanology. Volume 72, pages 1009-1020.

Martin, R.S., Sawyer, G.M., Day, J.A., LeBlond, J.S., Ilyinskaya, E., and Oppenheimer, C. (2012): High-resolution size distributions and emission fluxes of trace elements from Masaya volcano, Nicaragua; Journal of Geophysical Research: Solid Earth. Volume 117, pages.

Nriagu, J.O. and Becker, C. (2003): Volcanic Emissions of Mercury to the Atmosphere: Global and Regional Inventories; Science of The Total Environment. Volume 304, pages 3-12.

Pyle, D.M. and Mather, T.A. (2003): The importance of volcanic emissions for the global atmospheric mercury cycle; Atmospheric Environment. Volume 37, pages 5115-5124.

Witt, M.L.I., Mather, T.A., Pyle, D.M., Aiuppa, A., Bagnato, E., and Tsanev, V.I. (2008): Mercury and Halogen Emissions from Masaya and Telica Volcanoes, Nicaragua; Journal of Geophysical Research Solid Earth. Volume 113, Issue B6, 15 pages.

Zambardi, T., Sonke, J.E., Toutain, J.P., Sortino, F., and Shinohara, H. (2009): Mercury emissions and stable isotopic compositions at Vulcano island (Italy); Earth and Planetary Science Letters. Volume 277, pages 236-243.

Zelinski, M.E., Fischer, T.P., de Moor, J.M., Marty, B., Zimmermann, L., Ayalew, D., Nekrasov, A.N., and Karandashev, V.K. (2013): Trace elements in the gas emissions from the Erta Ale volcano Afar, Etheopia; Chemical Geology. Volume 357, pages 95-116.

Appendix 1: Atmospheric GEM data from each station, including parameters of each sample.

Station:	Sampler ID	Active/Passive	Collected Hg (ng)	Volume Sampled (m^3)	Atm. Conc. (ng m^{-F3})
Main Vent	CR1-A-1	Active	3.67	0.22	16.80
	CR1-A-2	Active	1.61	0.36	4.49
	CR1-A-3	Active	0.42	0.21	2.04
	CR1-P-1	Passive	7.58	0.95	8.02
	CR1-P-2A	Passive	4.94	0.95	5.22
	CR1-P-2B	Passive	6.85	0.95	7.24
	CR1-P-2C	Passive	4.88	0.95	5.16
Crater Rim	CR3-A-1A	Active	8.71	2.42	3.59
	CR4-A-1B	Active	9.47	2.42	3.90
	CR4-A-2	Active	43.70	13.84	3.12
	CR4-A-3	Active	1.19	0.63	1.90
	CR4-P-1A	Passive	3.18	1.22	2.61
	CR4-P-1B	Passive	3.67	1.22	3.02
	CR4-P-1C	Passive	3.35	1.22	2.76
	CR4-P-2A	Passive	2.84	0.95	3.00
	CR4-P-2B	Passive	2.96	0.95	3.13
	CR4-P-2C	Passive	2.01	0.95	2.12
	CR4-P-3	Passive	7.46	3.00	3.25
Sulfur Cone	CR2-A-1	Active	1.60	0.07	24.24
	CR2-P-1	Passive	7.21	0.95	8.51
	CR2-P-2A	Passive	8.44	0.95	8.93

	CR2-P-2B	Passive	12.2	0.95	12.91
	CR2-P-2C	Passive	8.37	0.95	8.86
Borbollón	CR3-A-1	Active	0.41	0.20	2.07
	CR3-P-1A	Passive	5.62	2.42	2.08
	CR3-P-1B	Passive	6.55	2.42	2.43
	CR3-P-2A	Passive	3.94	0.95	4.16
	CR3-P-2B	Passive	4.65	0.95	4.87
Permanent MultiGAS	CR5-P-1A	Passive	5.79	1.49	3.90
	CR5-P-1B	Passive	5.55	1.49	3.74
Mirador	CR6-A-1	Active	0.76	0.56	1.15
	CR7-P-1A	Passive	3.74	3.24	1.15
	CR7-P-1B	Passive	3.99	3.24	1.23
	CR7-P-1C	Passive	3.91	3.24	1.21
Field Blank	FB-A-1	Active	0.32	0	NA
Field Blank	FB-P-1	Passive	0.08	0	NA

Appendix 2: List of relevant volcanic information, including eruption frequency and Hg/SO_2 ratio from available literature

Volcano	Lat./Long.	Elev. (m)	Type	Eruptions. (200 yr.)	Hg/SO_2 ratio	Reference
Poás	10.2N/84.233W	2708	Stratovolcano	51	3.7E-8;4.9E-8	Bagnato et al., (2014)
Masaya	11.984N/86.161W	635	Caldera	31	2.00E-5	Witt et al., (2008)
Turrialba	10.025N/83.767W	3340	Stratovolcano	13	3.90E-6; 5.60E-6	Bagnato et al., (2014)
Vulcano	38.404N/14.962E	500	Stratovolcano	8	1.16E-7;2.4E-6	Ferrara et al., (2000); Aiuppa et al., (2007)
Miyakejima	34.094N/139.526E	775	Stratovolcano	15	9.00E-6	Bagnato et al., (2011)
Asama	36.406N/138.523E	2568	Complex	63	5.50E-6	Bagnato et al., (2011)
Nyiragongo	1.52S/29.25E	3470	Stratovolcano	20	5.50E-6	Bagnato et al., (2011)
Yasur	19.532S/169.447E	361	Stratovolcano	53	1.7E-5	Bagnato et al., (2011)
Ambrym	16.25S/168.12E	1334	Shield	3	6.40E-6	Bagnato et al., (2011)
Soufriere Hills	16.72N/62.18W	916	Stratovolcano	3	1.20E-5	Bagnato et al., (2011)
Stromboli	38.789N/15.213E	924	Stratovolcano	5	4.70E-6	Bagnato et al., (2011)
Etna	37.748N/14.999E	3295	Stratovolcano	112	7.1E-6;3.4E-6	Bagnato et al., (2014)
Gorely	52.559N/158.03E	1799	Caldera	15	3.30E-6	Bagnato et al., (2014)
Mutnovsly	52.449N/158.196E	2288	Complex	18	1.9E-7; 1.4E-5	Bagnato et al., (2014)
Aso	32.884N/131.104E	1592	Caldera	96	1.30E-6	Bagnato et al., (2014)
Rincon de la Vieja	10.83N/85.324W	1916	Complex	27	3.50E-6	Bagnato et al., (2014)
Kilauea	19.421N/155.287W	1222	Shield	63	1.60E-6	Mather et al., (2012); Varekamp and Buseck (1986)
Erebus	77.53S/167.17E	3794	Stratovolcano	15	20E-6	Wardell et al., (2008)
Colima	19.514N/103.62W	3850	Stratovolcano	37	2.50E-6	Varekamp and Buseck (1986)
St. Helens	46.2N/122.18W	2549	Stratovolcano	17	6.00E-6	Varekamp and Buseck (1981)
Mt. Hood	45.374N/121.695W	3426	Stratovolcano	6	7.10E-6	Varekamp and Buseck (1986)
Mt. Shasta	41.409N/122.193W	4317	Stratovolcano	0	3.90E-5	Varekamp and Buseck (1986)
White Island	37.52S/177.18E	321	Stratovolcano	41	2.90E-6	Wardell et al., (2008)

Appendix 3: Eruptions used for global volcanic Hg flux calculation

Volcano	Erupted SO_2 (kt)	Erupted SO_2 (t)	Eruptions (200yr)	Hg/SO_2 ratio from curve (eq 1)	Calculated Hg flux (t)
2015					
Telica	1	1000	34	5.86E-06	0.01
Kuchinoerabujima	4	4000	16	6.19E-06	0.02
Wolf	200	200000	10	6.31E-06	1.26
Fournaise, Pilon de la	2	2000	130	4.35E-06	0.01
Villarrica	5	5000	53	5.52E-06	0.03
Fournaise, Pilon de la	2	2000	130	4.35E-06	0.01
Manam	50	50000	37	5.80E-06	0.29
Zhupanovsky	10	10000	9	6.33E-06	0.06
Sheveluch	15	15000	19	6.14E-06	0.09
Ambrym	20	20000	3	8.92E-06	0.18
Chikurachki	5	5000	17	6.17E-06	0.03
Fuego	2	2000	32	5.89E-06	0.01
Fournaise, Pilon de la	3	3000	130	4.35E-06	0.01
Soputan	2	2000	37	5.80E-06	0.01
Etna	25	25000	112	4.60E-06	0.11
Momotombo	1.5	1500	11	6.29E-06	0.01
Fournaise, Pilon de la	2	2000	130	4.35E-06	0.01
Cotopaxi	20	20000	42	5.71E-06	0.11
Calbuco	400	400000	13	6.25E-06	2.50
					4.78
2014					
Ontakesan	1	1000	4	7.31E-06	0.01
Sheveluch	5	5000	19	6.14E-06	0.03
Turrialba	3	3000	10	6.31E-06	0.02
Fogo	382	382000	8	6.36E-06	2.43
Pavlof	46	46000	41	5.73E-06	0.26
Sangeang Api	100	100000	18	6.15E-06	0.62
Pacaya	2	2000	13	6.25E-06	0.01
Fournaise, Piton de la	1	1000	130	4.35E-06	0.00
Zhupanovsky	227	227000	9	6.33E-06	1.44
Pavlof	10	10000	41	5.73E-06	0.06
Sinabung	20	20000	2	1.34E-05	0.27
Kelut	200	200000	17	6.17E-06	1.23

Hunga Tonga-Hunga Ha'apai	14	14000	5	6.72E-06	0.09
Bardarbunga	11800	11800000	5	6.72E-06	79.32
Rabaul	31	31000	15	6.21E-06	0.19
					85.99
2013					
Etna	10	10000	112	4.60E-06	0.05
Klyuchevskoy	55	55000	88	4.95E-06	0.27
Klyuchevskoy	2	2000	88	4.95E-06	0.01
Etna	40	40000	112	4.60E-06	0.18
Cleveland	1	1000	21	6.10E-06	0.01
Pavlof	5	5000	41	5.73E-06	0.03
Etna	5	5000	112	4.60E-06	0.02
Paluweh	40	40000	8	6.36E-06	0.25
San Miguel	5	5000	34	5.86E-06	0.03
Veniaminof	5	5000	21	6.10E-06	0.03
Etna	7	7000	112	4.60E-06	0.03
Manam	10	10000	37	5.80E-06	0.06
					0.97
2012					
Soputan	10	10000	37	5.80E-06	0.06
Fuego	2	2000	32	5.89E-06	0.01
San Cristobal (Nicaragua)	5	5000	25	6.02E-06	0.03
Bezymianny	3	3000	52	5.54E-06	0.02
Tolbachik	200	200000	25	6.02E-06	1.20
Etna	31	31000	112	4.60E-06	0.14
Etna	6.5	6500	112	4.60E-06	0.03
Etna	1.1	1100	112	4.60E-06	0.01
San Cristobal (Nicaragua)	1	1000	25	6.02E-06	0.01
Copahue	500	500000	13	6.25E-06	3.13
Soputan	2	2000	37	5.80E-06	0.01
Tongariro	1	1000	70	5.24E-06	0.01
					4.65
2011					
Hudson, Cerro	1	1000	4	7.31E-06	0.01
Etna	4.8	4800	112	4.60E-06	0.02
Nyamuragira	1719	1719000	46	5.64E-06	9.70
Grimsvotn	300	300000	24	6.04E-06	1.81
Etna	6	6000	112	4.60E-06	0.03
Planchon-Peteroa	1	1000	14	6.23E-06	0.01
Nabro	3650	3650000	1	2.59E-05	94.57
Puyehue-Cordon Caulle	200	200000	10	6.31E-06	1.26

Etna	52.7	52700	112	4.60E-06	0.24
Soputan	10	10000	37	5.80E-06	0.06
Tengger Caldera	24	24000	58	5.44E-06	0.13
Kirishimayama	30	30000	30	5.93E-06	0.18
Etna	7	7000	112	4.60E-06	0.03
Kizimen	23	23000	2	1.34E-05	0.31
Bulusan	1.2	1200	21	6.10E-06	0.01
Etna	8	8000	112	4.60E-06	0.04
Zubair Group	1	1000	3	8.92E-06	0.01
Gamalama	8	8000	43	5.70E-06	0.05
Soputan	2	2000	37	5.80E-06	0.01
Etna	5	5000	112	4.60E-06	0.02
					108.49
2010					
Sheveluch	11	11000	19	6.14E-06	0.07
Fournaise, Piton de la	1	1000	130	4.35E-06	0.00
Tengger Caldera	5	5000	58	5.44E-06	0.03
Merapi	300	300000	52	5.54E-06	1.66
Pacaya	23	23000	13	6.25E-06	0.14
Fournaise, Piton de la	1	1000	130	4.35E-06	0.00
Nyamuragira	601	601000	46	5.64E-06	3.39
Soufriere Hills	30	30000	3	8.92E-06	0.27
Tengger Caldera	12	12000	58	5.44E-06	0.07
Kizimen	37	37000	2	1.34E-05	0.50
Eyjafjallajokull	466	466000	2	1.34E-05	6.24
					12.37
2009					
Redoubt	159	159000	6	6.50E-06	1.03
Manda Hararo	34	34000	2	1.34E-05	0.46
Sarychev Peak	1200	1200000	14	6.23E-06	7.48
Soufriere Hills	8	8000	3	8.92E-06	0.07
Bezymianny	1	1000	52	5.54E-06	0.01
Koryaksky	2	2000	6	6.50E-06	0.01
Fernandina	521	521000	26	6.00E-06	3.13
Llaima	10	10000	50	5.57E-06	0.06
		0			**12.24**
2008		0			
Soputan	16	16000	37	5.80E-06	0.09
Alu-Dalafilla	150	150000	1	2.59E-05	3.89
Azul, Cerro	157	157000	11	6.29E-06	0.99
Etna	46.5	46500	112	4.60E-06	0.21
Chaiten	14	14000	1	2.59E-05	0.36
Soputan	33	33000	37	5.80E-06	0.19
Soufriere Hills	3	3000	3	8.92E-06	0.03
Chikurachki	20	20000	17	6.17E-06	0.12

Okmok	150	150000	15	6.21E-06	0.93
Llaima	30	30000	50	5.57E-06	0.17
Soufriere Hills	5	5000	3	8.92E-06	0.04
Kasatochi	2000	2000000	1	2.59E-05	51.82
					58.85
2007					
Tair, Jebel at	80	80000	4	7.31E-06	0.58
Etna	12	12000	112	4.60E-06	0.06
Soputan	12	12000	37	5.80E-06	0.07
Bezymianny	5	5000	52	5.54E-06	0.03
Etna	10	10000	112	4.60E-06	0.05
Krummel-Garbuna-Welcker	1	1000	3	8.92E-06	0.01
Bulusan	1	1000	21	6.10E-06	0.01
Etna	10.5	10500	112	4.60E-06	0.05
Fuego	2	2000	32	5.89E-06	0.01
Chikurachki	30	30000	17	6.17E-06	0.19
Bulusan	1	1000	21	6.10E-06	0.01
Gamkonora	1	1000	11	6.29E-06	0.01
Fuego	2	2000	32	5.89E-06	0.01
Karthala	0.6	600	31	5.91E-06	0.00
Soufriere Hills	1	1000	3	8.92E-06	0.01
Fuego	2	2000	32	5.89E-06	0.01
Chikurachki	20	20000	17	6.17E-06	0.12
Soputan	5	5000	37	5.80E-06	0.03
Manda Hararo	26	26000	2	1.34E-05	0.35
Klyuchevskoy	176	176000	88	4.95E-06	0.87
Etna	6	6000	112	4.60E-06	0.03
Lopevi	12	12000	30	5.93E-06	0.07
Bulusan	0.5	500	21	6.10E-06	0.00
Fournaise, Piton de la	300	300000	130	4.35E-06	1.30
					3.87
2006					
Fourpeaked	1	1000	1	2.59E-05	0.03
Rabaul	300	300000	15	6.21E-06	1.86
Nyamuragira	675	675000	46	5.64E-06	3.81
Etna	9.3	9300	112	4.60E-06	0.04
Karthala	10	10000	31	5.91E-06	0.06
Cleveland	0.13	130	21	6.10E-06	0.00
Soufriere Hills	200	200000	3	8.92E-06	1.78
Bezymianny	5	5000	52	5.54E-06	0.03
Bulusan	1	1000	21	6.10E-06	0.01
Merapi	10	10000	52	5.54E-06	0.06
Tungurahua	10	10000	9	6.33E-06	0.06
Augustine	10	10000	8	6.36E-06	0.06

Manam	50	50000	37	5.80E-06	0.29
Tinakula	2	2000	19	6.14E-06	0.01
Soputan	10	10000	37	5.80E-06	0.06
Fournaise, Piton de la	1	1000	130	4.35E-06	0.00
Tungurahua	30	30000	9	6.33E-06	0.19
Home Reef	25	25000	3	8.92E-06	0.22
Lascar	2	2000	29	5.95E-06	0.01
Barren Island	0.2	200	9	6.33E-06	0.00
					8.59

Annual average (tonnes per year)	**30.08**
Standard deviation (annual averages)	**39.46**